5. Halocarbons and other Atmospheric Trace Species

B.D. HALL (EDITOR), J.H. BUTLER, A.D. CLARKE, G.S. DUTTON, J.W. ELKINS, D.F. HURST, D.B. KING, E.S. KLINE, J. LIND, L.T. LOCK, D. MONDEEL, S.A. MONTZKA, F.L. MOORE, J.D. NANCE, E.A. RAY, P.A. ROMASHKIN, AND T.M. THOMPSON

5.1. OVERVIEW

The mission of the Halocarbons and other Atmospheric Trace Species (HATS) group is to study halocarbons and other trace gases that cause chemical and radiative change in the atmosphere. The goal of HATS is to measure and interpret the distributions and trends of these species in the troposphere, stratosphere, and ocean with the best analytical instrumentation available. The species measured include nitrous oxide (N_2O); many halogenated species, such as halocarbons, fluorocarbons, perfluorocarbons (PFCs), and sulfur hexafluoride (SF_6); organic nitrates, such as peroxyacetyl nitrate (PAN); organic sulfur gases, such as carbonyl sulfide (COS); and hydrocarbons (HCs). The halocarbons include the chlorofluorocarbons (CFCs); chlorocarbons (CCs), such as CCl_4, CH_3CCl_3, $CHCl_3$, CH_2Cl_2, and C_2Cl_4; hydrochlorofluorocarbons (HCFCs); hydrofluoro-carbons (HFCs); methyl halides (CH_3Br, CH_3Cl, and CH_3I); bromocarbons (CH_2Br_2 and $CHBr_3$); and halons.

Three primary research areas involving these trace gases are stratospheric ozone depletion, climate change, and air quality. For example, the CFCs and N_2O are major ozone-depleting and greenhouse gases. The trace gas SF_6 is a greenhouse gas with a large global warming potential, but its net warming is small because of its low concentration in the atmosphere. Short-lived halocarbons, PAN, and the HCs play an important role in global and regional pollution. PAN is a major precursor of tropospheric ozone in the remote marine atmosphere. Tropospheric COS is a relatively stable sulfur molecule that contributes to the stratospheric aerosol layer.

Research conducted by HATS in 2000 and 2001 included (1) weekly flask sampling and analysis of air from remote and continental-influenced sites, (2) operation of instrumentation for hourly, in situ measurements of trace gases at the four CMDL baseline observatories, Barrow Observatory (BRW), Mauna Loa Observatory (MLO), Samoa Observatory (SMO), and South Pole Observatory (SPO), and at four continental-influenced sites, (3) preparation and maintenance of trace gas standards, (4) participation on airborne campaigns with in situ gas chromatographs (GCs) on aircraft and balloon payloads, (5) investigation of oceanic processes that influence trace gas composition of the atmosphere, and (6) measurement of many trace gases in firn air from South Pole.

Continuing programs within HATS are based upon in situ and flask measurements of the atmosphere from the 4 CMDL baseline observatories and 10 cooperative stations (Figure 5.1). Table 5.1 lists the geographic locations and other useful information for all the sites. There are currently 14 flask sites and 8 in situ sampling sites in the HATS atmospheric sampling network.

One of the highlights of this report is that the total equivalent chlorine (Cl + Br) in the troposphere continues to decrease at about 1% yr^{-1} as a result of the Montreal Protocol [*UNEP*, 1987]. Total equivalent chlorine in the stratosphere appears to have leveled off or peaked at most altitudes. The main reason for the decline in the troposphere is that methyl chloroform (CH_3CCl_3) concentrations continued to decline to less than half of the peak levels present in 1992. However, atmospheric concentrations of the halons and CFC-12 are still increasing because of permitted production in the developing countries and the large bank of chemicals that exists in the developed countries. As a result of the halon increase, the total bromine in the troposphere and stratosphere is still increasing. Once atmospheric CH_3CCl_3 is depleted, the trend in total equivalent chlorine may significantly change, requiring further observation.

Other significant results include the global increases in atmospheric N_2O and SF_6, observed from both flask and in situ monitoring, the continued growth of the CFC replacements (HCFCs and HFCs), and the decline in the northern hemispheric concentrations of $CHCl_3$ and C_2Cl_4 as a result of the U.S. Clean Air Act. Carbonyl sulfide distributions from both in situ and flask measurements are described for the first time and show a strong seasonal cycle. A new flask station was added in 2001 at Trinidad Head, California. Airborne measurements were conducted in the upper troposphere and lower stratosphere in the northern polar region during the 1999 and 2000 Stratospheric Aerosol and Gas Experiment III (SAGE III) Ozone Loss and Validation Experiment (SOLVE) conducted from Kiruna, Sweden. The rapid-sampling airborne gas chromatograph was also used to measured CFCs, halons, and chlorinated solvents in Russia along the trans-Siberian railway during June-July 2001 in a collaboration with Russian and German scientists. The construction of the next-generation airborne GC with electron capture and mass spectrometric detection was funded by the National Aeronautics and Space Administration (NASA) Instrument Incubation Program to measure trace gases, including hydrocarbons and organic nitrates, that influence atmospheric chemistry in the upper troposphere. An in situ GC system, equipped with one mass selective detector and two electron capture detectors, is being built for the new U.S. West Coast sampling site (Trinidad Head, California, or elsewhere on the U.S. West Coast) to monitor pollution originating in Asia and transported over the Pacific Ocean.

5.2. CONTINUING PROGRAMS

5.2.1. FLASK SAMPLES

Overview

Arrangements were made in 2001 to add two new stations to the sampling network. One of these is an additional remote site in the far southern hemisphere, located at

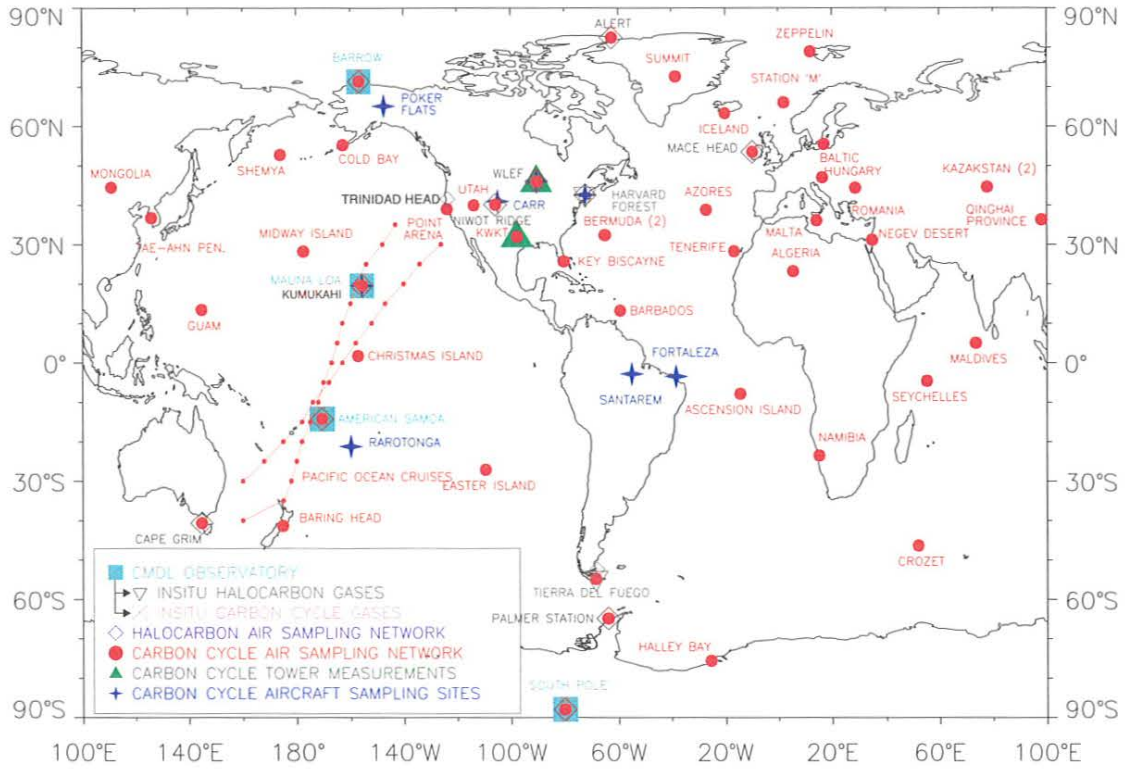

Fig. 5.1. Geographic locations of stations in the CMDL/HATS flask and in situ networks, along with CMDL/Carbon Cycle Greenhouse Gases (CCGG) stations (N_2O and SF_6 collected in glass flasks) and tower sites (triangles, future in situ halocarbon measurement).

TABLE 5.1. Geographic and Network Information for HATS Network Sites

Code	Station	Latitude	Longitude	Elevation (m)	LST – GMT (h)	Type
ALT	Alert, Northwest Territories, Canada*	82.45°N	62.52°W	210	-4	F
BRW	Point Barrow, Alaska	71.32°N	136.60°W	11	-9	F, I
MHD	Mace Head, Ireland (University College)	53.33°N	9.90°W	42	0	F
LEF	WLEF tower, Wisconsin (CMDL/CCGG)	45.95°N	90.28°W	470	-6	F, I
HFM	Harvard Forest, Massachusetts (Harvard University)	42.54°N	72.18°W	340	-5	F, I
THD	Trinidad Head, California (Humbolt State University)	41.05°N	124.15°W	109	-8	F
NWR	Niwot Ridge, Colorado (University of Colorado)	40.04°N	105.54°W	3013	-7	F, I
ITN	WITN tower, North Carolina (CMDL/CCGG)†	35.37°N	77.39°W	9	-5	F, I
MLO	Mauna Loa, Hawaii	19.54°N	155.58°W	3397	-10	F, I
KUM	Cape Kumukahi, Hawaii	19.52°N	154.82°W	3	-10	F
SMO	Tuluila, American Samoa	14.23°S	170.56°W	77	-11	F, I
CGO	Cape Grim, Tasmania, Australia‡	40.41°S	144.64°E	94	+10	F
TDF	Ushuaia, Argentina (WMO GAW station)§	54.82°S	68.32°W	10	-3	F, I
PSA	Palmer Station, Antarctica¶	64.92°S	64.00°W	10	+12	F
SPO	South Pole, Antarctica	89.98°S	102.00°E	2841	+12	F, I

F, flasks; I, in situ.
*Cooperative site with Environment Canada.
†Site's flask and in situ GC instrument closed down on June 12, 1999.
‡Cooperative site with Commonwealth Scientific and Industrial Research Organization (CSIRO) and Bureau of Meteorology, Australia.
§Began collecting data in November 2001.
¶Only glass flasks used.

Ushuaia, near Tierra del Fuego (TDF), Argentina (Figure 5.1, Table 5.1). This is a cooperative site with the Argentine government and is a Global Atmospheric Watch (GAW) station sponsored by the World Meteorological Organization (WMO). The second site, located at Trinidad Head, California (THD), is considered a regional sampling site and has been established for evaluating regional-scale air quality. It is anticipated that Trinidad Head will receive a mix of air from over the remote ocean and from nearby forests and small towns. It also may be useful for detecting air masses transported from Asia. Sampling at Mace Head, Ireland (MHD), was suspended for almost a year, as flasks began disappearing in transit. Biweekly sampling at MHD was reinitiated near the end of 2001. Efforts to improve sampling frequency and precision at all sites have continued throughout 2000-2001.

Flasks brought into the laboratory are analyzed on two to four instruments, depending upon the species being examined and the size of the individual sampling flask (Table 5.2). Analyses are performed by a gas chromatograph with electron capture detection (GC-ECD) and/or a gas chromatograph with mass spectrometric (GC-MS) detection. Although all 300-ml flasks have been retired, there still remain some 850-ml flasks, which contain a marginal amount of air for all of these low-level analyses. Most flask analyses are of samples from the network, although many are from research cruises, firn air sampling, and other special projects. One hundred new electropolished, stainless-steel flasks were recently purchased from Lab Commerce (formerly known as Meritor Corporation, San Jose, California) to supply the new sites, to upgrade flask quality and quantity at old sites, and to use for special projects.

In 1996, 269 flasks from the network were filled and delivered to the Boulder laboratory for analysis. This number has increased each year, reaching a total of 415 in 2000 (Figure 5.2). This increase is the result of added sites and more efficient turnover of flasks between Boulder and the field sites. This was accomplished through improved record keeping of flasks coming to Boulder and by addition of flasks to the network. Sampling success has steadily improved from that for 1996 at all sites (Table 5.3). This was mainly the result of small leak repairs and valve replacements on flasks, where necessary. These repairs greatly improved the agreement in flask pressure between simultaneously sampled pairs (Figure 5.3).

GC-ECD Results

CFC-12 continues to increase in the atmosphere; however, it may have leveled off in the northern hemisphere (Figure 5.4). Mixing ratios of CFC-11 continue to drop steadily (Figure 5.5). The CFC-11 growth rate (-1.75 ± 0.11 (95% C.L.) ppt yr^{-1}, 0.7% yr^{-1}) for 2000 through mid-2001 does not differ from the rate determined for 1997-

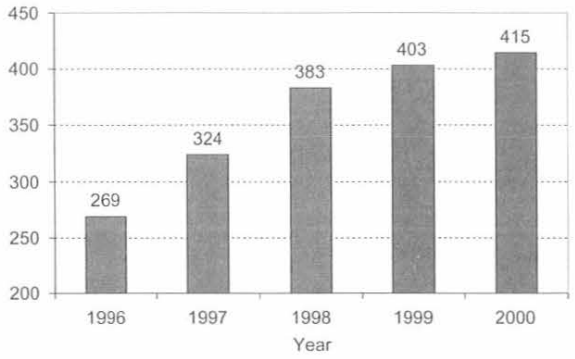

Fig. 5.2. Number of flask pairs filled and returned to Boulder each year from the HATS station network.

TABLE 5.2. Instrumentation for HATS Flask Analysis

Instrument	Type	Gases	Frequency of Network Data
OTTO	GC-ECD (three-channel, isothermal)	N_2O, CFCs (3), CCs (2), SF_6	Weekly
LEAPS	GC-ECD (one-channel, temperature–programmed)	Halons (2), CH_3Cl, CH_3Br, $CHCl_3$	Semimonthly to monthly
HCFC-MS	GC-MSD (one -channel temperature-programmed)	HCFCs (3), HFCs (1), CFCs (3), halons (1), CCs (6), BrCs (3), COS	Semimonthly
HFC-MS	GC-MSD (one -channel, temperature-programmed)	HCFCs (5), HFCs (2), CFCs (2), halons (2), CCs (6), BrCs (3), BrCCs (3)	Semimonthly to monthly

OTTO, not an acronym; LEAPS, Low Electron Attachment Potential Species; BrCs, bromocarbons; BrCCs, bromochlorocarbons.

TABLE 5.3. Percentage Sampling Success at CMDL Observatories and Cooperative Sampling Sites

Sampling Station	1996	1997	1998	1999	2000
Barrow, AK	69%	94%	88%	87%	90%
Mauna Loa, HI	69%	83%	90%	96%	94%
American Samoa	54%	67%	73%	88%	88%
South Pole	77%	69%	77%	88%	81%
Alert, Canada	52%	46%	67%	67%	65%
Niwot Ridge, CO	63%	92%	87%	77%	88%
Cape Grim, Australia	60%	69%	85%	87%	85%
WLEF tower, WI	12%	35%	69%	92%	100%
Harvard Forest, MA	46%	62%	69%	69%	88%
Kumukahi, HI	50%	54%	67%	69%	83%
Palmer, Antarctica	—	8%	65%	81%	96%
Mace Head, Ireland*	—	—	8%	15%	—
WITN tower, NC†	65%	62%	62%	38%	—

Sampling success is defined as the fraction of flasks analyzed relative to the number expected (i.e., one pair per week).

*Sampling was discontinued temporarily in 2000 because of loss of flasks in shipments.

†Site was discontinued indefinitely in 1999.

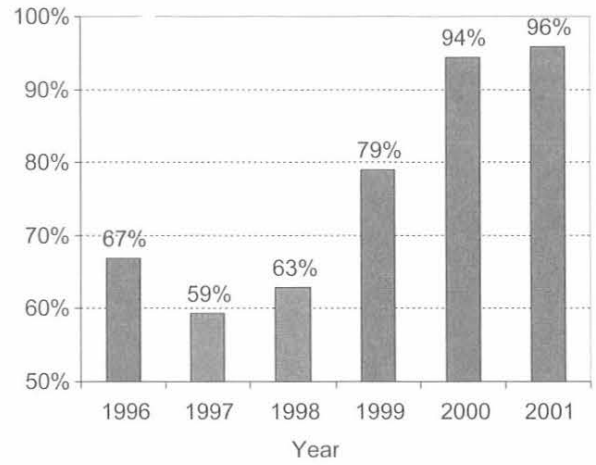

Fig. 5.3. Percentage of flask pairs agreeing within 1 psi in total pressure upon arrival in Boulder.

2001 (-1.73 ± 0.03 ppt yr^{-1}). CFC-113 and CCl_4 are also both decreasing, at about 1% yr^{-1}. The global growth rate of N_2O (Figure 5.6) during 1978-2000 was 0.74 ± 0.01 ppb yr^{-1}, which amounts to a mean of about 0.25% yr^{-1}. During 1999 through mid-2001, the global growth rate was 0.73 ± 0.06 ppb yr^{-1}, which does not differ from the 23-yr average. Sulfur hexafluoride (Figure 5.7) still appears to be increasing linearly in the atmosphere, with a growth rate of about 0.22 ± 0.01 ppt yr^{-1} since 1996.

The mixing ratios of halons are still increasing slowly in the atmosphere, in spite of a ban on their production in developed countries as of 1994. The global growth rate of halon-1301 (Figure 5.8) from 1999 through 2000 (0.06 ± 0.07 ppt yr^{-1}) does not differ significantly at the 95% confidence level from the 1995-2000 average of 0.06 ± 0.01 ppt yr^{-1}, nor from the1995-1996 average of 0.044 ± 0.011 ppt yr^{-1} reported in *Butler et al.* [1998]. The growth rate of halon-1211 (Figure 5.9) seems to be slowing, having dropped from a steady rate of 0.16 ± 0.02 ppt yr^{-1} in the late 1980s and early 1990s to 0.094 ± 0.04 ppt yr^{-1} for 1999 through mid-2001.

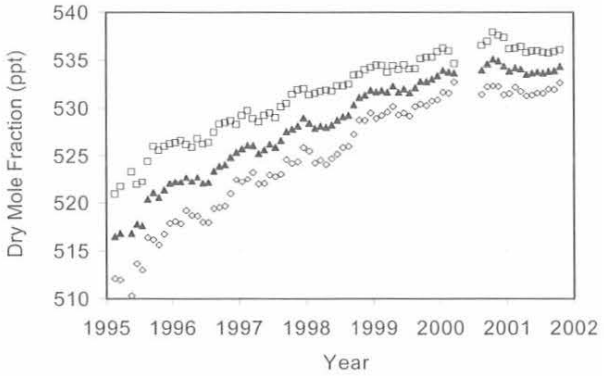

Fig. 5.4. Recent measurements of CFC-12 in the atmosphere. Measurements are monthly averages of GC-ECD data: northern hemisphere means (squares), global means (triangles), and southern hemisphere means (diamonds).

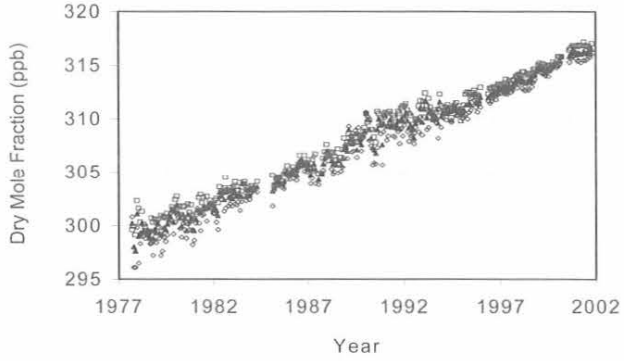

Fig. 5.6. Atmospheric history of N_2O since 1977 (GC-ECD monthly means; symbols as in Figure 5.4). A new GC-ECD instrument has been used since 1994.

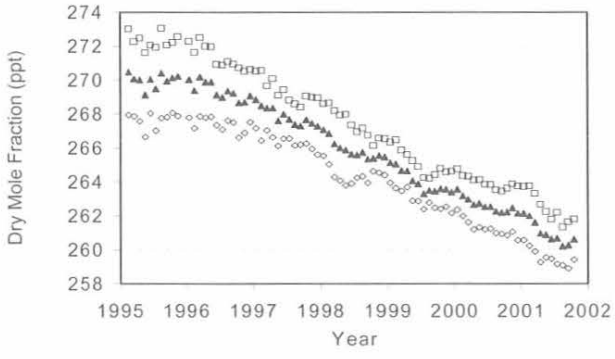

Fig. 5.5. Recent measurements of CFC-11 in the atmosphere showing a steady loss rate since 1997 (GC-ECD monthly means; symbols as in Figure 5.4).

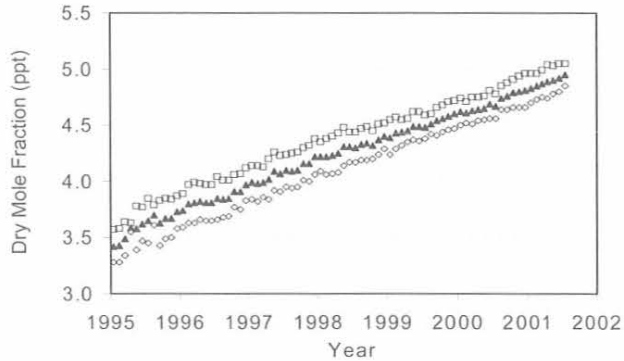

Fig. 5.7. Recent history of atmospheric SF_6 from CMDL flask measurements (GC-ECD monthly means; symbols as in Figure 5.4).

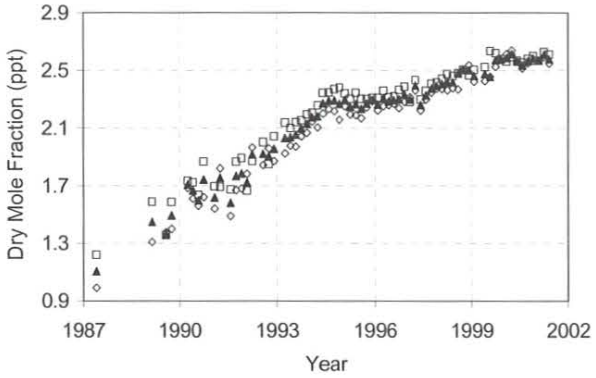

Fig. 5.8. Atmospheric history of halon-1301 (GC-ECD bimonthly averages; symbols as in Figure 5.4).

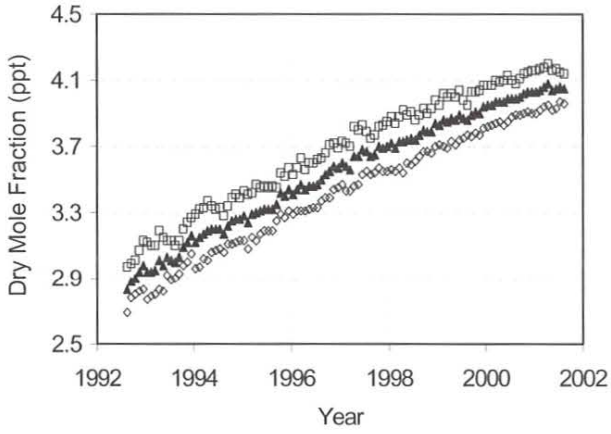

Fig. 5.9. Recent atmospheric history of halon-1211 (GC-MSD monthly means; symbols as in Figure 5.4).

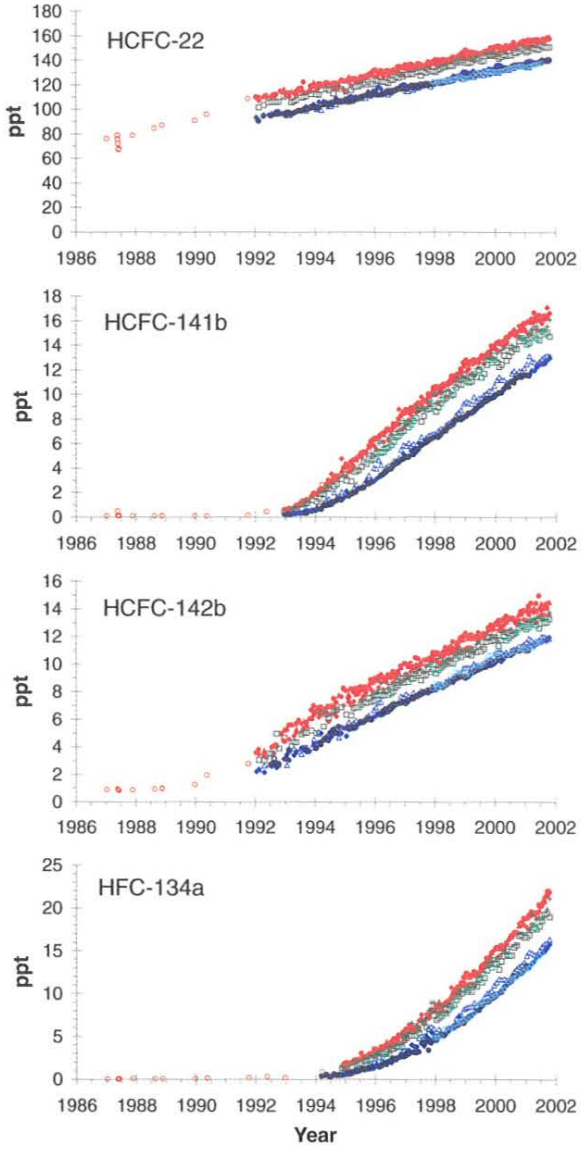

Fig. 5.10. Atmospheric dry mole fractions (ppt) of selected HCFCs and HFC-134a measured by GC-MSD in the CMDL flask program. Each point represents monthly means at one of eight or nine stations: ALT, BRW, NWR, red; KUM, MLO, green; SMO, CGO, PSA, SPO, blue. Also plotted are results from analysis of archived air samples (open red circles) filled at NWR and in past cruises from both hemispheres.

GC-MS Results

Chlorofluorocarbons alternatives measurement program. Measurements of CFC alternatives and other trace gases were continued during 2000-2001 from flasks collected at 12 locations. In both years, three samples per month, on average, were filled and analyzed on GC-MSD instrumentation at 11 of the 12 sites. Fewer samples from MHD were collected and analyzed owing to difficulties associated with shipping.

Tropospheric mixing ratios of HCFCs and HFCs continued to increase during 2000-2001 (Figure 5.10, Table 5.4). Fairly linear rates of increase have been observed for HCFC-22, HCFC-141b, HCFC-142b, and HFC-134a since 1998. By mid-2001, chlorine in the three most abundant HCFCs amounted to nearly 190 ppt, or almost 7% of all chlorine carried by long-lived, purely anthropogenic halocarbons. Total chlorine from the HCFCs increased at between 8 and 9 ppt yr^{-1} over this period. Despite rapid relative growth observed for HFC-134a during the mid-1990s, a fairly constant rate of increase of 3.2 ppt yr^{-1} has been observed since 1998 (Table 5.4).

Atmospheric methyl chloroform. Atmospheric mixing ratios of methyl chloroform (1,1,1-trichloroethane, CH_3CCl_3) continue to decline exponentially (Figure 5.11).

TABLE 5.4. Global Burden (Mixing Ratio) and Rate of Change of HCFCs and HFC-134a

Compound	Mean 2000 (ppt)	Mean 2001 (ppt)	Growth Rate (ppt yr^{-1})
HCFC-22	141.6	146.3	5.0 (1992-2001)
HCFC-141b	12.7	14.0	1.7 (1998-2001)*
HCFC-142b	11.7	12.5	1.0 (1998-2001)*
HFC-134a	13.8	17.2	3.2 (1998-2001)

Quantities are estimated from latitudinally weighted measurements at seven remote stations: SPO, CGO, SMO, MLO, NWR, BRW, and ALT.

* Slower growth is indicated in 2000-2001 (0.1-0.2 ppt yr^{-1} less than shown).

During 2000 through mid-2001, the growth rate of CH_3CCl_3 declined at about 18% yr^{-1}. The exponential decay time constant has been consistent at 5.5 ± 0.1 yr since the beginning of 1998, and continues to provide an upper limit to the global lifetime of CH_3CCl_3 in the atmosphere [*Montzka et al.*, 2000]. If it is presumed those emissions of CH_3CCl_3 have not changed substantially from that estimated for 1998-1999 [*Montzka et al.*, 2000; *Prinn et al.*, 2001], then these results continue to suggest a global lifetime for CH_3CCl_3 of 5.2 years (for the years 1998-2001). In contrast to estimates of CH_3CCl_3 lifetime for the years before 1995, this lifetime estimate is very insensitive to calibration uncertainties. It is still sensitive, however, to the magnitude of present-day emissions.

Slightly shorter estimates of methyl chloroform lifetime have been reported by *Prinn et al.* [2001] for the period 1978-2000. They suggest, however, that the methyl chloroform lifetime has changed over time. They also estimate a lifetime longer than 5.0 years in the later 1990s, which is reasonably consistent with 5.2 years in 1998-2001. The outstanding question with regard to this issue is understanding this apparent change in lifetime. Does it stem from inaccurate estimates of emissions, decreases in OH in recent years, or a change in the true lifetime of methyl chloroform that is unrelated to OH?

The hemispheric difference has not changed substantially since 1998; for the years 1998-2001, the hemispheric difference is estimated to be 2.8 (±0.4)%. This difference is similar at all sampling stations at comparable latitudes in the two hemispheres: 2-3% in the tropics deduced from SMO, MLO, and KUM data; 2-3% in midlatitudes deduced from CGO, NWR, and LEF data; and 2-4% in polar regions deduced from PSA, SPO, BRW, and ALT data (see Table 5.1 for station definitions and locations). The constancy in both the decay time constant and the hemispheric difference suggests that the influence of emissions on estimates of global lifetime and hemispheric lifetimes has either been small or relatively constant since 1998.

Overall trends in ozone-depleting gases. Ground-based measurements provide an indication of the burden and trend of individual ozone-depleting gases. The sum of chlorine and bromine atoms in long-lived trace gases provides an estimate of equivalent tropospheric chlorine (ETCl) after

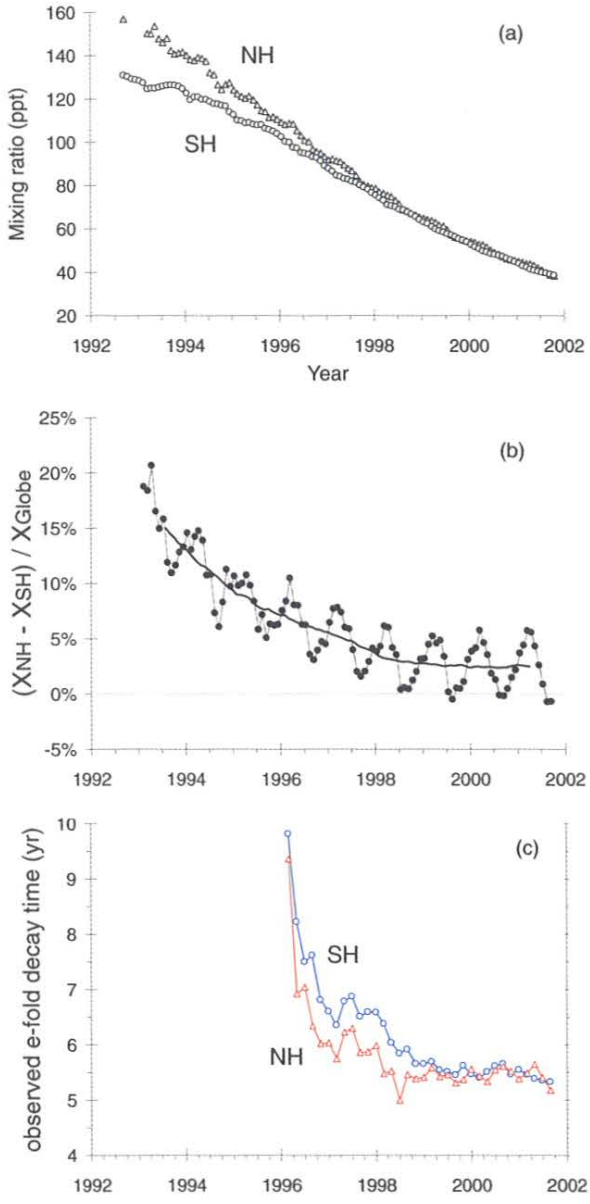

Fig. 5.11. (a) Atmospheric dry mole fractions (ppt) of CH_3CCl_3 measured by GC-MSD in the CMDL flask program. Each point represents a monthly hemispheric surface mean as determined by a latitudinal weighting of results from individual sampling stations (northern hemisphere = triangles, southern hemisphere = circles). (b) The hemispheric mixing ratio difference for CH_3CCl_3 at the Earth's surface in recent years. The difference was inferred from weighted, monthly mean mixing ratios at three to six sampling stations in each hemisphere. Monthly differences (solid circles) are connected with a thin line; the heavy curve represents a 12-mo running mean difference. (c) The observed e-fold decay time for monthly hemispheric surface means of CH_3CCl_3 shown in (a). A fairly constant exponential decay in surface mixing ratios of CH_3CCl_3 has been observed since the beginning of 1998; the exponential time constant for this decay is 5.5 years.

the enhanced efficiency of bromine to destroy ozone compared with chlorine is included (a factor of 50 is used here; *Solomon et al.* [1995]). ETCl provides an indication of the upper limit to ozone-depleting chlorine and bromine in the future stratosphere. Better approximations of trends in inorganic halogen in the lower stratosphere can be derived from ETCl after accounting for the different rates at which halocarbons photo-oxidize in the stratosphere. These rates have been estimated empirically or with models and are applied as weighting factors to mixing ratios of individual gases in the calculation of effective equivalent chlorine (EECl) and effective equivalent stratospheric chlorine (EESC) [*Daniel et al.*, 1995; *Montzka et al.*, 1996]. The only difference between EECl and EESC is that EESC explicitly includes a 3-yr time lag (dates associated with EECl correspond to the time when the surface measurement was made).

The net sum of ozone-depleting halogen from purely anthropogenic gases continued to decrease during 2000-2001 (Figure 5.12). The rates of decline for EECl and ETCl in 2001 were about 1% yr^{-1} and 0.5% yr^{-1}, respectively. Amounts of EECl during mid-2001 were about 5.5% below the peak observed near the beginning of 1994. The rate of decline in both EECl and ETCl has slowed by about one-third compared with peak values as the influence of methyl chloroform has diminished.

The two scenarios for EECl and ETCl shown in Figure 5.12 provide some insight into causes of past changes and the future evolution of net halogen in the atmosphere. The measured trends in EECl and ETCl since 1998 have remained fairly close to scenario A, in which constant emissions were presumed [*Montzka et al.*, 1999]. Although substantial reductions in emissions were realized during the 1990s, these results suggest that these emission reductions have slowed in recent years, perhaps owing to enhanced CFC production in developing countries.

The updated projections for scenario B (Figure 5.12, solid lines) are somewhat different from the ones made previously (see references noted in Figure 5.12). The main difference arises from consideration of halons in the future. In the present calculation it has been assumed halon emissions will decrease in future years in reasonable accord with reported halon production [*Fraser et al.*, 1999] and a small allotment for additional future production.

Shorter-lived gases. Measurements of other chlorinated and brominated trace gases were continued during 2000-2001 (Figure 5.13). The results suggest further decreases in mixing ratios of CH_2Cl_2 and C_2Cl_4. Interannual variability is observed for the methyl halides and will be discussed in future publications.

Non-stainless-steel flasks circulated to sampling stations. Although most samples are routinely collected in stainless-steel flasks in the HATS program, glass flasks have also been used recently. Glass flasks are particularly useful when known artifacts affect sampling in steel flasks. Glass flasks sampled during the South Pole 2000 winter allowed for additional measurements of compounds that undergo substantial degradation in stainless-steel flasks during the long period between sampling and analysis (Figure 5.14). Glass flasks are also useful to determine if results for more reactive gases are independent of flask type. Preliminary

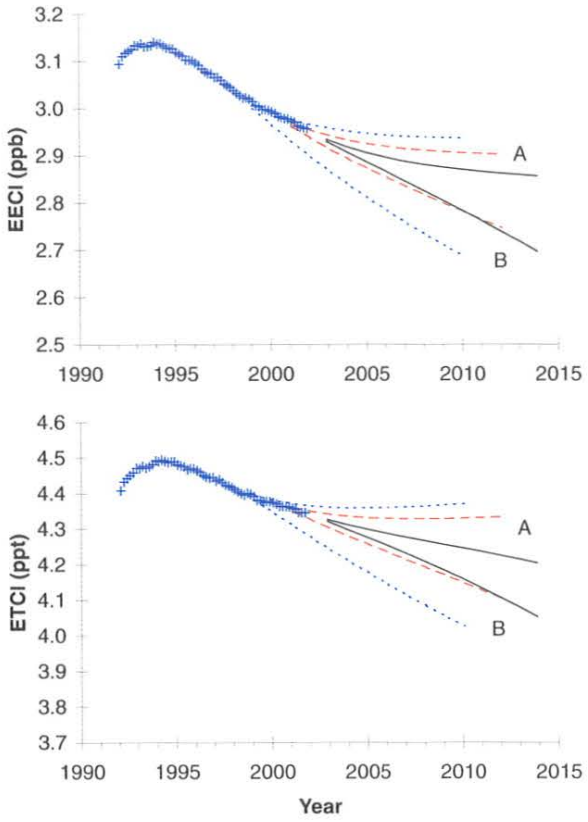

Fig. 5.12. The measured and potential future burden of ozone-depleting halogen in the lower atmosphere. Ozone-depleting halogen is estimated from tropospheric measurements of anthropogenic halocarbons by appropriate weighting factors to calculate effective equivalent chlorine (EECl) for midlatitudes (top) and equivalent tropospheric chlorine (ETCl) as an upper limit for polar latitudes (bottom) [*Daniel et al.*, 1995; *Montzka et al.*, 1996, 1999]. A constant offset was added to account for CH_3Cl and CH_3Br. Projections are based on two limiting scenarios: A, emissions of all long-lived halogenated gases (CFCs, HCFCs, CH_3CCl_3, CCl_4, and halons) remain constant at 2001 levels, and B, scenario A with the exception that emissions of CFCs, CH_3CCl_3, halons, and CCl_4 continue decreasing at 5 to 8% yr^{-1}. Future scenarios have been formulated in previous *CMDL Summary Reports* and other publications with ambient air measurements through 1997 (short-dashed lines [*Montzka et al.*, 1999]) and through 1999 (long-dashed lines [*Hall et al.*, 2001]). Updates to current emission rates and their rates of change based on measurements through 2001 were used to update projections for both scenarios (solid lines).

results of glass flasks filled at CGO and SPO show good consistency for HCFC-22, HCFC-142b, and HFC-134a. Glass flasks are not without problems for some compounds, however. Poor consistency is observed for HCFC-141b and C_2Cl_4 in glass flasks; this contamination probably is associated with the Teflon seals in these flasks and does not suggest trouble in results reported from stainless-steel flasks for these gases.

Carbonyl sulfide. Measurements of carbonyl sulfide (COS) were begun from flasks during 2000-2001. COS is

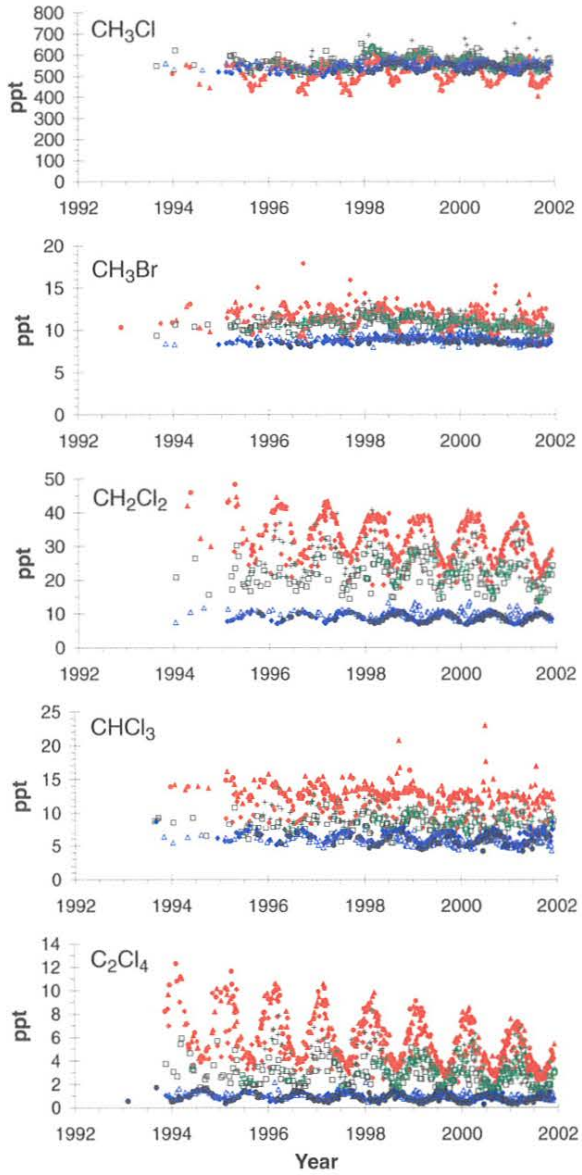

Fig. 5.13. Atmospheric dry-air mole fractions (ppt) determined for selected chlorinated trace gases and CH_3Br by GC-MSD in the CMDL flask program. Each point represents the mean of two simultaneously filled flasks from one of eight or nine stations (symbols the same as in Figure 5.10). Results shown for all compounds except C_2Cl_4 are from 2.4-L stainless-steel flasks only.

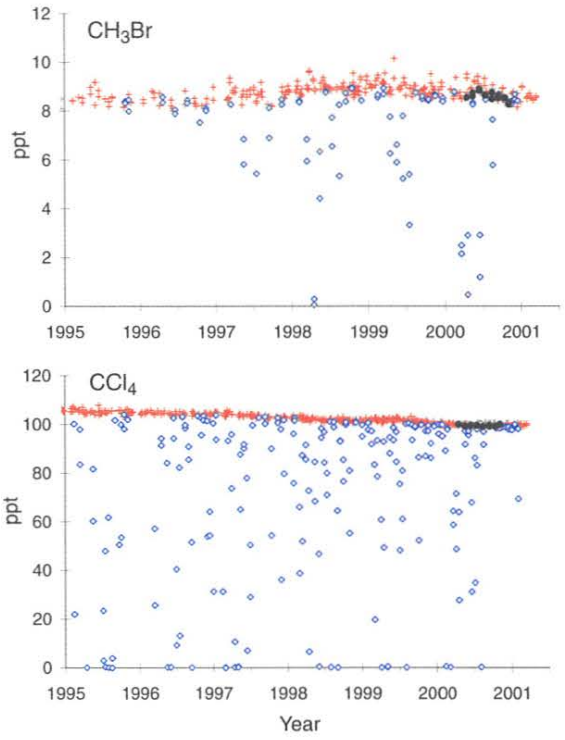

Fig. 5.14. Mixing ratios determined from different sites and different types of flasks. Results for CH_3Br and CCl_4 from Cape Grim, Tasmania (40°S), from stainless-steel flasks (red pluses) are compared with data obtained from South Pole from stainless-steel flasks (open blue diamonds) and glass flasks (solid black circles).

an abundant sulfur-containing gas that is believed to contribute significantly to the sulfur found in the stratosphere. More recent model calculations, however, have suggested a lesser role for COS in maintaining the stratospheric aerosol than was previously thought [*Kjellström*, 1998].

The results from flasks show a small hemispheric difference biased slightly toward higher levels in the southern hemisphere, strong seasonal variations at all sites except SMO, and seasonality in the two hemispheres that is not 180 days out of phase (Figure 5.15). These features are also evident in data from Chromatograph for Atmospheric Trace Species (CATS) GC-ECD instrumentation located at selected sites. Many conflicting reports regarding hemispheric distributions and seasonality can be found in the current literature for COS. These observations will add substantially to the understanding of the global budget of this gas.

5.2.2. In Situ Gas Chromatograph Measurements

Radiatively Important Trace Species

The Radiatively Important Trace Species (RITS) project has ended. Table 5.5 outlines, for each station and data channel, the shutoff dates for the RITS equipment. Channel A measured N_2O, CFC-12 (CCl_2F_2), and CFC-11 (CCl_3F); channel B measured CFC-11, CH_3CCl_3, and CCl_4; and channel C measured N_2O. The RITS instruments continued to collect data until data from the replacement CATS instruments showed similar trends and equal or better precision. The precision for a particular chemical was

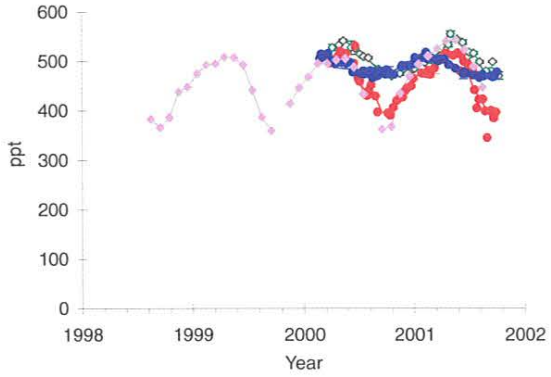

Fig. 5.15. Mixing ratios for COS determined from sampling and analysis of stainless-steel flasks at BRW (red), KUM (green), and CGO (blue). Also shown are monthly means at BRW from the on-site CATS GC-ECD (purple diamonds). For clarity, SMO data are not shown.

determined as the standard deviation of the ratio of the responses of two calibration gases over an extended period of time (usually more than 1 month). Calibration gases are normally very stable for the species of interest.

Instruments associated with the CATS project, developed to replace the aging RITS instruments and add new measurement capabilities, continue to operate at the CMDL field sites. A CATS system was installed at NWR in October 2000. Table 5.6 shows the installation dates for the CATS instruments and the duration of the RITS-CATS comparisons.

A two-channel Hewlett-Packard 5890 GC-ECD used in the RITS project was refurbished for installation at Ushuaia, Tierra del Fuego, Argentina (TDF), as part of a cooperative venture with the Servicio Meteorologico Nacional de Argentina, sponsored by WMO. The TDF site is part of the WMO GAW program. This GC measures N_2O and SF_6 on the first channel and CFC-12, CFC-11, CFC-113, CH_3CCl_3, and CCl_4 on the second channel. A significant difference between this system and the previous RITS system is that nitrogen carrier gas with a CO_2 dopant is used on the N_2O-SF_6 channel as opposed to 5% CH_4 in argon (P-5). The use of CO_2-doped N_2 should (a) eliminate any CO_2 interference

TABLE 5.5. RITS Project Shutdown Schedule

Station	Channel*	Date and Time (GMT)
BRW	A, B, C	Feb. 17, 1999 (2100)
NWR	A, B, C	Aug. 7, 2001 (1900)
MLO	A, C	April 10, 2000 (2130)
	B	Dec. 18, 2000 (2030)
SMO	A, B	April 22, 2000 (0530)
	C	Sept. 30, 2000 (0000)
SPO	A, B	Nov. 30, 2000 (0200)

* See text for channel definitions.

TABLE 5.6. CATS Project Startup and Overlap Schedule with RITS

Station	Installation Date	Overlap with RITS (months)
BRW	June 16, 1998	8
NWR	Oct. 13, 2000	10
MLO	Sept. 29, 1998	18 [26]*
SMO	Dec. 4, 1998	17 [22]*
SPO	Jan. 30, 1998	34

*Months in brackets are for the one channel that continued to be operated after the others were turned off.

on the N_2O signal and (b) improve carrier gas quality (high-quality P-5 is difficult to obtain, particularly at remote sites).

The TDF GC system was installed on October 26, 2001, providing the first in situ CFC measurements in South America. Scientists from Argentina are interested in measuring CFCs because stratospheric chlorine from CFCs contributes to the formation of the Antarctic ozone hole. During vortex breakup, low-ozone events can occur over southern South America. Furthermore, while the total atmospheric chlorine burden is dropping [*Montzka et al.*, 1999; *Elkins*, 2000], CFC-12 is slowly increasing. Under the *Montreal Protocol on Substances that Deplete the Ozone Layer* [*UNEP*, 1987] and its amendments, developing countries can produce CFCs until 2010.

Mixing Ratio Calculation Methods

Over the past 3 years the RITS three-channel GC instruments at the CMDL baseline observatories have been replaced by four-channel GC instruments (CATS). In addition to the five trace gases measured by RITS instruments (N_2O, CFC-11, CFC-12, CH_3CCl_3, and CCl_4), CATS instruments measure SF_6, CFC-113, $CHCl_3$, COS, halon-1301, halon-1211, CH_3Cl, CH_3Br, HCFC-142b, and HCFC-22.

Both RITS and CATS instruments are calibrated using two calibration tanks that are sampled alternately along with ambient air. One calibration standard (C1) consists of a mixture of 90% ambient air and 10% synthetic ultrapure air. The other standard (C2) is 100% ambient air. The sequence of sample injections is C1, A1, C2, A2, where A1 and A2 are ambient air samples obtained at two different heights on the sampling tower. Each sample chromatograph is 30 minutes in length; thus the full sequence takes 2 hours. Both RITS and CATS in situ measurement programs have utilized several different methods to compute the trace gas concentrations in air samples bracketed by two calibration samples. This section focuses on the difficulties involved in these calculations. A new algorithm, designed to minimize problems associated with calibration tank changes and uncertainties in the assignment of calibration tank mixing ratios (see section 5.2.3), is presented here.

One-point method. The simplest method of calculating mixing ratios is to use only one calibration tank as a reference measurement:

$$\chi_a = \frac{R_a}{R_c}\chi_c \quad , \tag{1}$$

where R_a is the ECD response of the air sample, R_c is the ECD response of the calibration sample, χ_c is the known mixing ratio of the calibration sample, and χ_a is the mixing ratio of the air sample. The one-point method can be plagued by nonlinearities in chromatography and detector response (Figure 5.16). Compounding problems occur when the calibration tank is replaced with a new tank with different assigned concentrations. Because the one-point method approximates the actual ECD response with a straight line with a zero intercept, a change in the mixing ratio of the calibration tank (χ_c and R_c) results in a different slope used to approximate the ECD response (Figure 5.16a). This can lead to discontinuities in the atmospheric record when the true ECD response is nonlinear. Small errors can occur even when two calibration tanks are used (i.e., mixing ratio is determined as the mean of two one-point calculations).

Two-point method. The results of both calibration tanks together can be used to calculate mixing ratios by approximation of the ECD response with a straight line with a nonzero intercept (Figure 5.17):

$$\chi_a = \frac{\left(R_a - R_{c1}\right)\left(\chi_{c1} - \chi_{c2}\right)}{R_{c1} - R_{c2}} + \chi_{c1} \quad , \tag{2}$$

where R_a is the ECD response of the air sample, R_{c1} is the ECD response of C1, R_{c2} is the ECD response of C2, χ_{c1} is the known mixing ratio of C1, and χ_{c2} is the known mixing ratio of C2. Improvements in accuracy, compared with the one-point method, can sometimes be obscured by precision problems associated with the two-point method. Random noise in both measured quantities R_{c1} and R_{c2} can affect the slope and intercept. Averaging calibration tank responses over short time periods can improve precision. Changing calibration tanks can also lead to discontinuities in the atmospheric record when the two-point method is used, because different segments of the nonlinear response curve are encountered as calibration tanks with different mixing ratios are used. This is particularly true for trace gases with strong tropospheric trends (such as CH_3CCl_3).

In addition to difficulties associated with nonlinear ECD response, the accuracies of both the one-point and two-point methods are dependent on the accuracies of the mixing ratios assigned to the calibration gases (χ_{c1} and χ_{c2}). To address these issues, a new method that utilizes the thousands of routine measurements made of each calibration tank during normal operation was developed. The method can be used to adjust assigned calibration tank concentrations (within specified uncertainties) to provide a self-consistent set of calibration standards and minimize discontinuities in the atmospheric time series.

Statistical ratio method. The CATS GCs make continuous measurements of each calibration tank every day, about 12 injections per day. Over the lifetime of the calibration tank (usually 9 to 12 months) nearly 4000 separate measurements of each calibration tank can be made. Several comparisons of one calibration tank to another (Figure 5.18) can be used to adjust the assigned mixing ratios such that the effects of calibration tank changes are minimized.

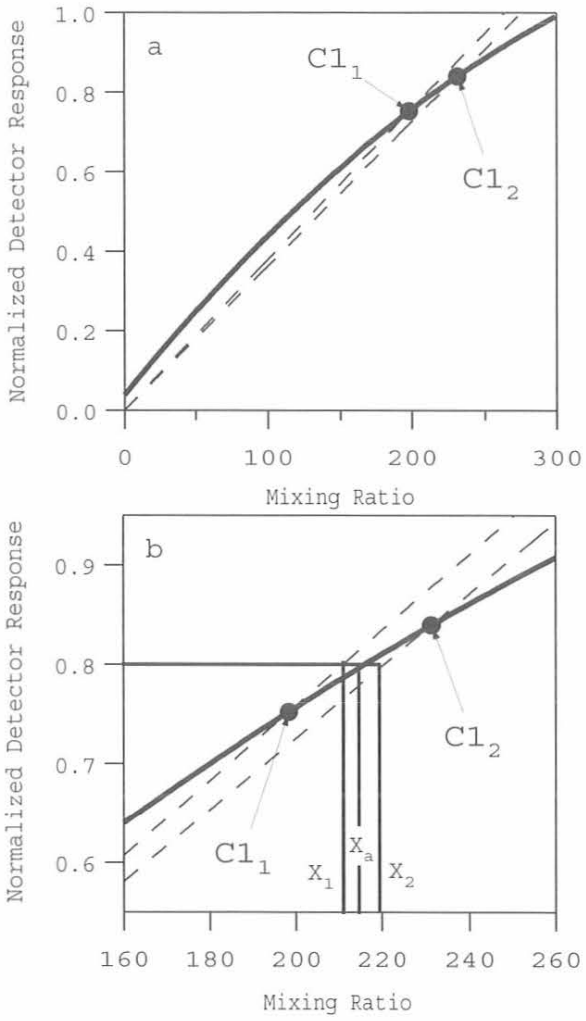

Fig. 5.16. Estimates of mixing ratio by the one-point method. Plot (a) is full scale and (b) is expanded. Both plots demonstrate the potential problems that can occur with only a single calibration measurement. The nonlinear response curve (solid) is the normalized response to a known quantity of a particular molecule (in arbitrary units). The one-point method uses a single measurement of an assigned mixing ratio ($C1_1$) and assumes a linear response (dotted lines). For an ECD with a nonlinear response, a calibration error will occur if the air sample and calibration gas have significantly different responses. The solid vertical lines (X_1, X_2) correspond to the mixing ratios calculated for a response of 0.8 using two different calibration standards ($C1_1$ and $C1_2$). The middle vertical line (X_a) is the actual mixing ratio if the response curve is known.

A two-step procedure is used to establish a self-consistent set of calibration tank mixing ratios. The first step takes advantage of the fact that the mean response ratio of calibration tanks is functionally related to the assigned calibration tank values:

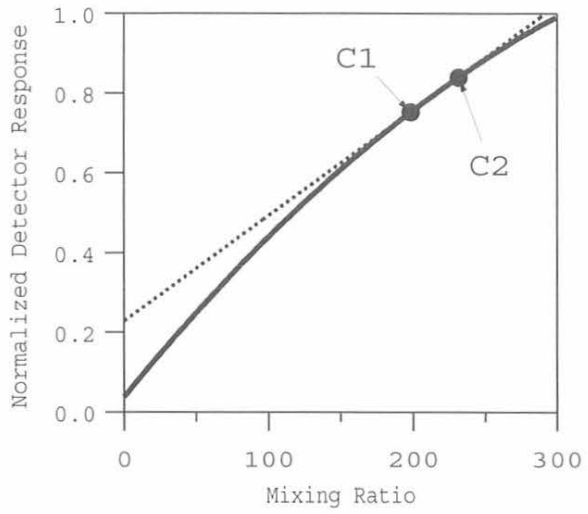

Fig. 5.17. Estimates of mixing ratio by the two-point method. This method utilizes two calibration tank measurements (C1 and C2) to approximate the response curve (solid) with a straight line (dashed).

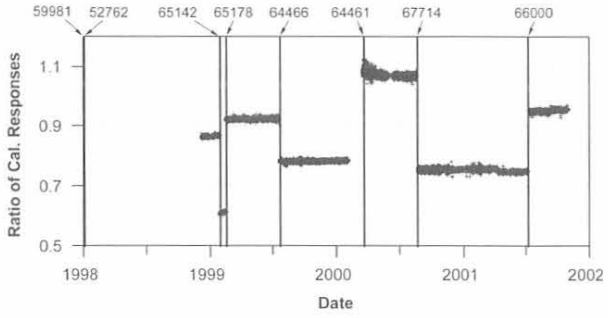

Fig. 5.18. Response ratio (C1/C2) for CH_3CCl_3 at SMO for different pairs of calibration standards. Calibration tank changes are shown as vertical lines identified by cylinder number along the top of the figure.

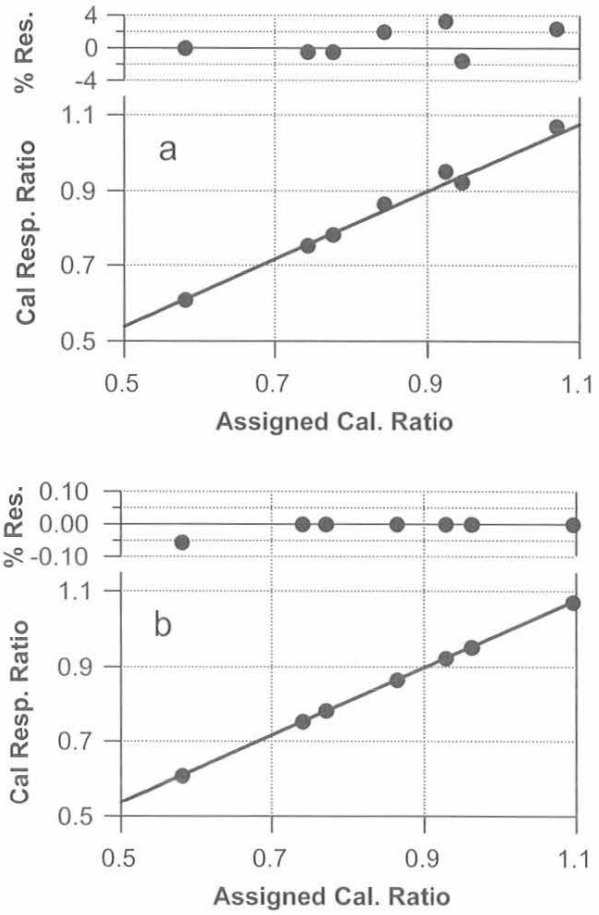

Fig. 5.19. (a) Mean response ratio for CH_3CCl_3 at SMO plotted against the ratio of assigned CH_3CCl_3 concentration for each calibration tank pair. A linear least-squares fit through the calibration tank ratios (solid line) is used to compute an average effective response curve. Residual differences are plotted at the top of the graph and demonstrate the magnitude of errors associated with a calibration tank change. (b) Mean response ratio as in (a) except that calibration tank concentrations have been adjusted to minimize the residuals.

$$B_{ij} = f\left(\chi_{c1,i}, \chi_{c2,j}\right) \approx m\left(\frac{\chi_{c1,i}}{\chi_{c2,j}}\right) + b \quad , \tag{3}$$

where B_{ij} is the response ratio of the i^{th} C1 tank to the j^{th} C2 tank, $\chi_{c1,i}$ is the assigned concentration for the i^{th} C1 tank, and $\chi_{c2,j}$ is the assigned concentration for the j^{th} C2 tank. The ratio B_{ij} can vary between 0.5 and 1.1 depending on the growth rate of the compound analyzed and when the calibration tanks were prepared. Plotting the measured mean calibration tank ratios (B_{ij}) versus assigned concentration ratios creates an effective ECD response curve (Figure 5.19a) that can be fitted with a least-squares regression line. The line represents a long-term average ECD response for a particular molecule. If the chromatography is stable over the period of all B_{ij} measurements, the linear fit can be used to calculate air concentrations and estimate errors. The functional relationship is nearly linear for all compounds measured by the CATS instruments. Problems arise in the linear representation when there are chromatographic problems, such as co-eluting compounds and ECD response curves that show relatively large nonzero intercepts. For current tropospheric mixing ratios of all species measured by CATS instruments, equation (3) seems to provide a good estimate for the effective response curve.

Once the slope and intercept of the effective response curve are known, uncertainties in the assigned calibration tank mixing ratios can be incorporated:

$$B_{ij} = m\left(\frac{\chi_{c1,i} + \sigma_{c1,i}}{\chi_{c2,j} + \sigma_{c2,j}}\right) + b \quad , \tag{4}$$

where $\sigma_{c1,i}$ is the possible uncertainty associated with the i^{th} C1 and $\sigma_{c2,j}$ is the possible uncertainty associated with the j^{th} C2. A numerical algorithm is used to iteratively adjust all $\sigma_{c1,i}$ and $\sigma_{c2,j}$ to minimize the residual difference (Figure 5.19b). The adjustments to the calibration tank values are constrained by the estimated uncertainties on the assigned values (section 5.2.3). For most compounds the adjustments are less than 0.5% of the ambient mixing ratio.

Equation (4) can be rewritten in terms of χ_a to yield two equations to compute atmospheric mixing ratio using the optimal values of $\sigma_{c1,i}$ and $\sigma_{c2,j}$:

$$\chi_a = (\chi_{c1,i} + \sigma_{c1,i})\, m \left(\frac{R_{c1,i}}{R_a} - b\right)^{-1} \quad , \tag{5}$$

$$\chi_a = (\chi_{c2,j} + \sigma_{c2,j}) \frac{1}{m} \left(\frac{R_a}{R_{c2,j}} - b\right) \quad . \tag{6}$$

If both calibration tanks are in operation, the average of equations (5) and (6) is used. Atmospheric mixing ratios calculated with the statistical ratio method tend to be more precise than with the two-point method and are more accurate than the one-point method. The gain in precision comes from use of the average response curve rather than estimation of a response curve from each sequence of measurements, as in the case of the two-point method.

Figures 5.20 and 5.21 illustrate the differences between results from the two-point method and from the statistical ratio method. Figure 5.20a shows discontinuities in the mixing ratio for CH_3CCl_3 at SMO calculated with the two-point method. These discontinuities are the result of rapidly changing atmospheric CH_3CCl_3 mixing ratios, and calibration tanks that have widely varying CH_3CCl_3 relative to the atmosphere. The CH_3CCl_3 data shown in Figure 5.20b were calculated with the statistical ratio method. These data clearly represent a continuous time series. The missing data seen prior to the 64461 calibration tank change correspond to a period in which the C2 tank (65178) was emptied before the arrival of its replacement. Even though the ratio of calibration tanks cannot be used for this period, the statistical relationship used to derive equations (5) and (6) is still valid. In this case the atmospheric mixing ratio can be calculated with equation (5) without having to rely on the one-point calculation method. The CFC-11 data from BRW shown in Figure 5.21 do not show large discontinuities associated with calibration tank changes. However, application of the statistical ratio method reveals a possible downward trend in CFC-11 concentration (Figure 5.21b) that is not apparent in data computed with the two-point method (Figure 5.21a).

The application of the statistical ratio method is new to the HATS in situ program and may undergo further enhancements. For example, the two-point method may be preferred during periods when chromatography is

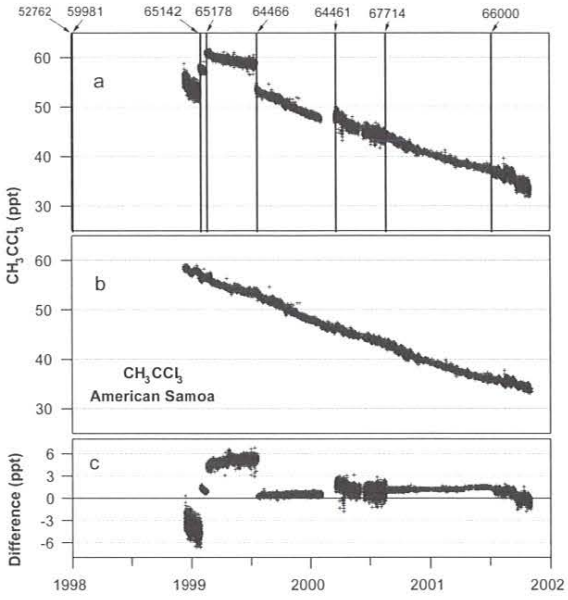

Fig. 5.20. CH_3CCl_3 data from SMO computed with two different methods: (a) the two-point method and (b) the statistical ratio method. The difference between methods (a) and (b) is shown in (c). Note that many of the discontinuities in (a) are absent in (b). Calibration tank changes are shown as vertical lines identified by cylinder number along the top of (a).

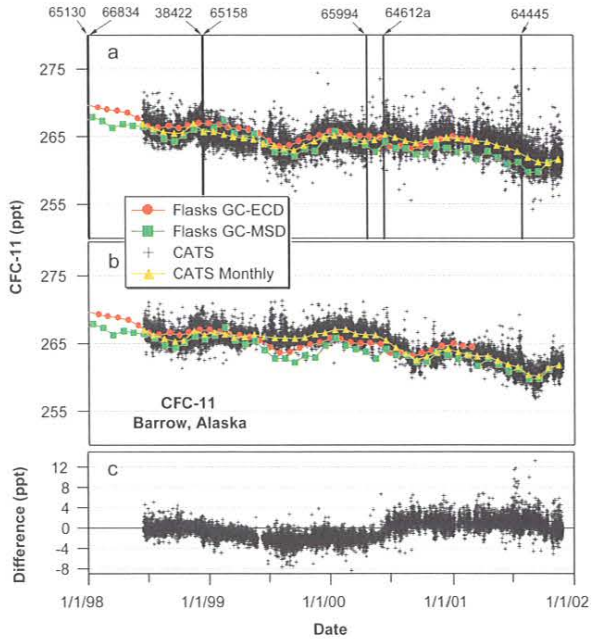

Fig. 5.21. CFC-11 data from BRW, as in Figure 5.20. Also included are data from flasks analyzed on GC-ECD (red) and GC-MSD (green) instruments, and monthly mean values from the CATS instrument (yellow). Although discontinuities are not apparent in (a), the statistical ratio method (b) dramatically improves precision.

noticeably different from the statistics upon which the method is based. However, with each additional working standard, the entire data record could change significantly when the statistical ratio method is applied. A future improvement might be to use equation (2) in conjunction with the estimated $\sigma_{c1,i}$ and $\sigma_{c2,j}$ for these periods.

5.2.3. GRAVIMETRIC STANDARDS

Calibration Scales

Numerous standards were prepared in 2000-2001. In total, 62 gravimetric standards were prepared and 89 working standards were filled at NWR during this period.

The calibration scales of N_2O, SF_6, CFC-12, CFC-11, CH_3CCl_3, CCl_4, and halon-1211 were examined with the aim of incorporating all HATS measurements, as well as CCGG N_2O and SF_6 flask measurements, on common scales. This involved analysis of numerous working standards used by the flask programs, airborne programs, and in situ programs. This work will continue into the near future and will include additional molecules.

A key element of this work involved the preparation of additional gravimetric standards for N_2O and SF_6 (Figures 5.22 and 5.23). Previous scales for these molecules had been defined by a limited number (four to six) of gravimetric

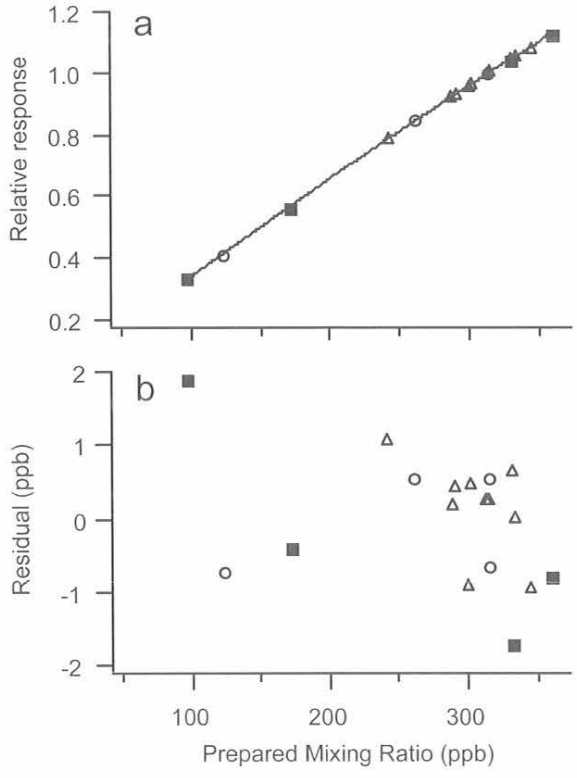

Fig. 5.22. (a) Second-order calibration curve and (b) residual, resulting from analysis of gravimetric standards that define the 2000 N_2O scale. Standards prepared from similar primary standards are shown as similar symbols.

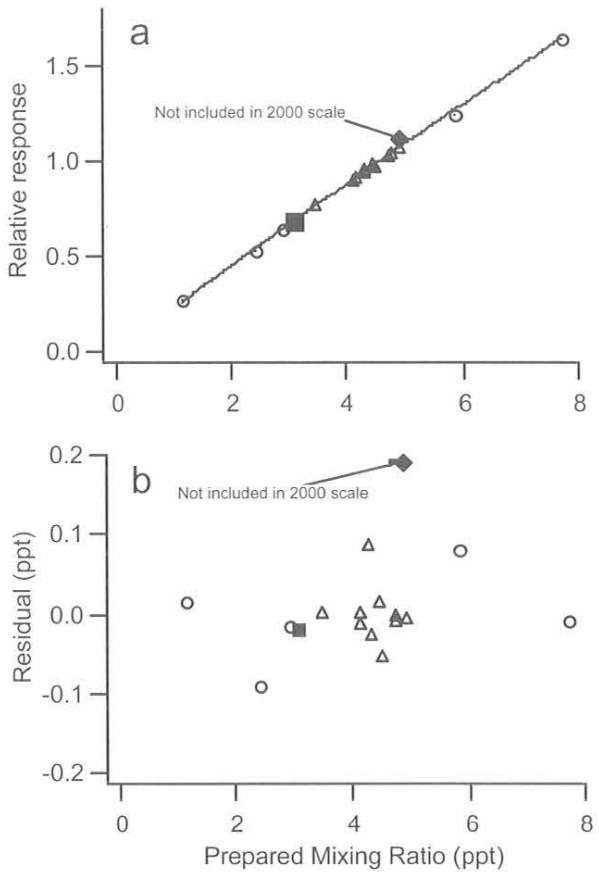

Fig. 5.23. (a) Second-order calibration curve and (b) residual, resulting from analysis of gravimetric standards that define the 2000 SF_6 scale. Standards prepared from similar primary standards are shown as similar symbols.

standards. While these standards were useful for defining a scale over a wide concentration range, the lack of multiple standards with near-ambient concentrations presented difficulties in establishing the long-term stability of these scales. New primary standards were prepared from the same reagents used to establish the original scales. Secondary/tertiary standards were prepared from the new primary standards as well as from existing primary standards. The 2000 N_2O scale is about 1 ppb lower than the 1993 scale, and it is 0.5 ppb higher than that predicted using 300 and 330 ppb National Institute of Standards and Technology (NIST) Standard Reference Materials (SRMs). The 2000 SF_6 scale differs from the 1994 scale [*Geller et al.*, 1997] by less than 0.1 ppt, which is within the uncertainty associated with the 1994 scale.

A scale based on a large number of standards makes it easier to identify outliers (standards that, for whatever reason, do not agree with the majority) (Figure 5.23). These new N_2O-SF_6 standards have also helped to improve the long-term stability of the N_2O and SF_6 scales (e.g., the loss or drift of a single standard does not affect the scale as much as it would if the scale were defined by only a few standards). More information on gravimetric standards used to define HATS scales,

including a list of the standards used to define the new 2000 N_2O and 2000 SF_6 scales, is available on the CMDL/HATS website (http://www.cmdl.noaa.gov/hats/standard/scales.htm).

A second element of this work involved the analysis of reagent-grade materials used to prepare primary standards. The reagents used to prepare primary CH_3CCl_3, CCl_4, and CFC-12 standards were sent to NIST (Gaithersburg, Maryland) for purity analysis. No significant volatile impurities were found in CFC-12 or CCl_4 reagents. However, the CH_3CCl_3 reagent used to establish the 1996 CH_3CCl_3 scale [see *Hall et al.*, 2001] was found to contain impurities amounting to approximately 6.4% (by mole). New high-purity reagent-grade CH_3CCl_3 was purchased from a different vendor (Sigma-Aldrich, St. Louis, Missouri.). The purity of this new reagent is approximately 99.8% based on the NIST analysis (99.9% according to the manufacturer's assay). New primary standards were prepared from this reagent. These new standards show a molar response that is roughly 5% higher than those prepared from the old reagent, which is consistent with the results of the reagent analysis. Development of a new CH_3CCl_3 scale is under way. It is expected that this new scale will be about 5% lower than the 1996 scale used in the publications of *Hurst et al.* [1997], *Volk et al.* [1997], *Butler et al.* [1999], *Montzka et al.* [1999, 2000], and *Romashkin et al.* [1999].

Gravimetric standards for carbonyl sulfide (COS) were prepared from newly purchased COS reagent. Several ppt-level standards were prepared in 29-L Aculife-treated aluminum cylinders. The stability of these standards is being evaluated. Two of five ppt-level standards are already showing signs of COS loss. Although many of the working standards used in the in situ program do not show COS loss, the viability of aluminum cylinders for COS at the ppt level is still being evaluated.

New gravimetric standards for CO were prepared in 1999-2000. These new standards helped to confirm that secondary standards prepared in 1989 had drifted and that a scale update was needed [*Tans et al.*, 2001]. The scale will be maintained by preparation of new gravimetric standards every 2 years and by comparison of ppb-level standards to ppm-level NIST SRMs.

Calibration of Working Standards

Working standards continue to be calibrated using a four-channel gas chromatograph similar to those used for in situ measurements (CATS). The initial calibration of this instrument was established in 1999 by comparison of a working standard (natural air at ambient concentration) to gravimetric standards, as well as to previous working standards. Routine calibration is maintained by comparison of the working standard to five additional working standards (mixtures of natural and ultrapure air at concentrations ranging from 40% to 100% of ambient). These comparisons are performed every 1-2 months or after a significant change in GC operating parameters. Frequent analysis of these working standards enables detection of small changes in GC performance or response characteristics without depletion of gravimetric standards. Each set of gravimetric standards used to define a particular scale is analyzed yearly.

The routine analysis of the working standards also provides information on the day-to-day variability of the GC. This information can be used to provide an estimate of the uncertainties associated with the calibration of working standards using this instrument. Knowledge of the day-to-day variability is crucial if small changes (drift) are to be detected. Table 5.7 shows the precision over a single day and uncertainties over multiday periods, associated with the calibration of a working standard. The information in Table 5.7 is related only to the performance of the CATS instrument and does not describe the accuracy of the calibration scales. It is useful to assess how well two identical standards can be calibrated, or the degree to which two calibrations of the same standard, performed months or years apart, can be expected to agree (assuming that the standard is stable over this period). Instrument precision on a given day (Table 5.7) is often very good, 0.4 ppb for N_2O, for example. However, differences in the mean concentration determined on different days can occur because of the imprecise nature of the calibration method and small changes in response characteristics associated with changes in carrier gas purity, column condition, etc. For these reasons, standards are typically analyzed on 2-3 different days. Uncertainties associated with multiday calibrations are larger than the daily precision and decrease with additional analysis, as expected. Although it is impractical to analyze working standards over 10 days, these data provide an estimate of the best overall uncertainty achievable with the CATS calibration system.

New High-Pressure Cylinders

Aluminum cylinders are not ideal for the long-term storage of methyl halides. Air stored in Aculife-treated aluminum cylinders, particularly those purchased since 1998, tend to show decreases of CH_3Br and increases in CH_3Cl over time. The rate of change of these compounds is highly variable and cylinder specific. A small number of these cylinders seem to be relatively stable, but an alternative is clearly needed.

TABLE 5.7. Precision and Uncertainties Associated with the Calibration of Working Standards

	Precision*	Uncertainty (3 days)†	Uncertainty (10 days)†
N_2O (ppb)	0.4	0.8	0.5
CFC-12 (ppt)	0.8	1.3	0.8
CFC-11 (ppt)	0.6	1.0	0.6
CFC-113 (ppt)	0.2	0.5	0.3
CH_3CCl_3 (ppt)	0.2	0.6	0.3
CCl_4 (ppt)	0.2	0.7	0.4
SF_6 (ppt)	0.03	0.04	0.02
Halon-1211 (ppt)	0.02	0.03	0.02

*Typical daily precision (expressed as $2\sigma/N^{0.5}$) associated with 8-10 comparisons of an unknown to a reference standard at ambient concentration. These data are similar to those of *Hall et al.* [2001].

†Uncertainties associated with a multiday calibration (95% confidence level). The uncertainties associated with the 3-day calibration are typical for the calibration of working standards used in the flask and in situ programs.

In an attempt to obtain gas cylinders that will be superior to aluminum cylinders for the long-term storage of methyl halides, several electropolished, stainless-steel cylinders were purchased. These cylinders are approved by the Department of Transportation for transport at pressures of 6200 kPa (900 psi). Preliminary stability testing involved filling cylinders with moist ultrapure air and moist natural air. No significant changes were observed in the ultrapure air samples (i.e., outgassing of compounds normally detected with CATS instruments was not observed).

5.3. AIRBORNE PROJECTS

The Airborne Chromatograph for Atmospheric Trace Species (ACATS-IV) [*Romashkin et al.*, 2001] and Lightweight Airborne Chromatograph Experiment (LACE) [*Moore et al.*, 2002] are GC instruments designed to measure CFCs, N_2O, SF_6, and other trace gases aboard aircraft (ACATS-IV and LACE) and balloon (LACE) platforms. Measurements of these trace gases in the lower stratosphere can provide insight into the chemistry and transport of that region. This section describes some of the science results deduced from measurements made during the Stratospheric Aerosol and Gas Experiment III (SAGE III) Ozone Loss and Validation Experiment (SOLVE) (with ACATS-IV and LACE) and the Atmospheric Chemistry and Combustion Effects Near the Tropopause II (ACCENT-II) campaign (with LACE).

SOLVE was an investigation of wintertime stratospheric ozone losses in the Arctic vortex using in situ and remotely sensed measurements made from aircraft and balloon platforms. The primary goal of SOLVE was to increase knowledge of the processes that influence northern polar ozone from late autumn through late winter. A second objective, validation of SAGE III ozone measurements, was not achieved because the satellite was not deployed prior to the campaign. SOLVE was conducted simultaneously with the Third European Stratospheric Experiment on Ozone 2000 (THESEO 2000), which included independent measurements from aircraft and balloons.

ACATS-IV was part of the NASA high-altitude ER-2 aircraft payload during the 2000 SOLVE campaign. The ER-2 aircraft flew 11 science flights from Kiruna, Sweden (67.9°N, 21.1°E), and 5 transit flight segments between Kiruna and NASA Dryden, Edwards, California, between January 9 and March 18, 2000. Science flights included deep vortex penetrations to 90°N, vortex edge and extra-vortex surveys, and multiple-level flights for vertical profiling. ACATS-IV produced science-quality data for each of these flights. As discussed by *Romashkin et al.* [2001], ACATS-IV was modified for SOLVE by decreasing the interval between measurements of N_2O, SF_6, CFC-12, and halon-1211 to 70 seconds, while CFC-11, CFC-113, $CHCl_3$, CH_3CCl_3, CCl_4, H_2, and CH_4 were measured every 140 seconds. *Romashkin et al.* [2001] also provided detailed information about the operation and calibration of ACATS-IV, the processing of data, and the precision and errors of measurements.

LACE was flown on two NASA-sponsored flights of the Observations of the Middle Stratosphere (OMS) balloon. The first flight, November 19, 1999, occurred just after the vortex edge had formed. The second flight, March 5, 2000, occurred just prior to vortex breakup.

Several significant alterations were made to the ER-2 payload for SOLVE. One important change was the replacement of the NASA Airborne Tunable Laser Absorption Spectrometer (ATLAS), a long-standing source of high-quality, 1-Hz N_2O data, with a new, compact, lightweight tunable diode laser spectrometer (Argus) designed to provide high-quality, 1-Hz N_2O data as well as high-precision measurements of CH_4 every 3 seconds. A comparison of coincident N_2O data from ACATS-IV, ATLAS, and the NASA Jet Propulsion Laboratory (JPL) Aircraft Laser Infrared Absorption Spectrometer (ALIAS) during two previous ER-2 campaigns [*Hurst et al.*, 2000] showed typical agreement of 1.9% between ACATS-IV and ATLAS, 2.7% between ACATS-IV and ALIAS, and 2.8% between ALIAS and ATLAS. A similar comparison of SOLVE N_2O data revealed typical agreement of 3.8% between ACATS-IV and Argus, 2.6% between ACATS-IV and ALIAS, and 4.0% between ALIAS and Argus [*Hurst et al.*, 2002]. The poorer agreement between N_2O instruments during SOLVE spawned the idea to construct a self-consistent, high-resolution N_2O data set from the data of the three in situ N_2O instruments. An objective statistical method was developed to reduce biases between the instruments, then combine their measurements into a "unified" N_2O data set with 3-s temporal resolution [*Hurst et al.*, 2002]. The quality of unified N_2O data was evaluated by integration of the data over the canister-filling periods of the National Center for Atmospheric Research (NCAR) Whole Air Sampler (WAS) during SOLVE ER-2 flights. The N_2O data from the canisters agree with the integrated unified N_2O data within about 1.5%, which is better than the agreement between any pair of N_2O instruments.

Record ozone losses for the Arctic stratosphere have been reported for winter 1999/2000 [*Richard et al.*, 2001; *Salawitch et al.*, 2002]. These losses are predominantly attributed to chemical O_3 destruction driven by the most widespread presence of polar stratospheric clouds (PSCs) in the Arctic since the 1970s [*Rex et al.*, 2002] and near-peak levels of total halogen (Cl + Br) in the lower stratosphere [*Elkins*, 2000]. Measurements of chlorinated and brominated source gases in the lower stratosphere, combined with CMDL surface measurements of these gases, attest to the high availability of inorganic halogen in the older air masses of the Arctic vortex. Figure 5.24 illustrates that organic chlorine (CCl_y) and organic bromine (CBr_y) are more than 50% converted to inorganic chlorine (Cl_y) and inorganic bromine (Br_y) in air masses with mean ages greater than 4.5 and 3.0 years, respectively. In addition, severe denitrification [*Popp et al.*, 2001] (Figure 5.25) greatly inhibited chlorine and bromine deactivation reactions that moderate O_3 destruction rates [*Gao et al.*, 2001]. *Fahey et al.* [2001] described the first in situ measurements of the large HNO_3-containing particles whose gravitational sedimentation resulted in the observed severe denitrification. In contrast, significantly dehydrated air masses (>10% H_2O loss) were rarely encountered between 17 and 21 km, indicating that temperatures in this altitude range were often below the temperature at which nitric acid trihydrate (NAT) forms, but seldom below the ice frost point. However, *Herman et al.* [2002] reported a slight decrease in total hydrogen with altitude that resulted from the widespread sedimentation of PSC particles during the winter.

Cumulative O_3 loss and O_3 loss rates in the Arctic vortex during SOLVE have been calculated from measurements made by instruments aboard the ER-2 aircraft and balloons. *Richard et al.* [2001] analyzed in situ data to determine a cumulative O_3 loss of 58 ± 4% at 19-km altitude between February 3 and March 12, 2000. Their calculations are based on the wintertime evolution of the vortex O_3:N_2O relationship (Figure 5.26a). Ozone loss rates at 19 km were as high as 51 ± 3 ppb d^{-1} during late winter (Figure 5.26b) [*Richard et al.*, 2001]. *Rex et al.* [2002] examined data from 770 O_3 sondes launched from 29 northern stations to sample distinct air masses twice over several day intervals as they circumnavigated the pole and reported 70% cumulative O_3 loss near 18-km altitude and a cumulative

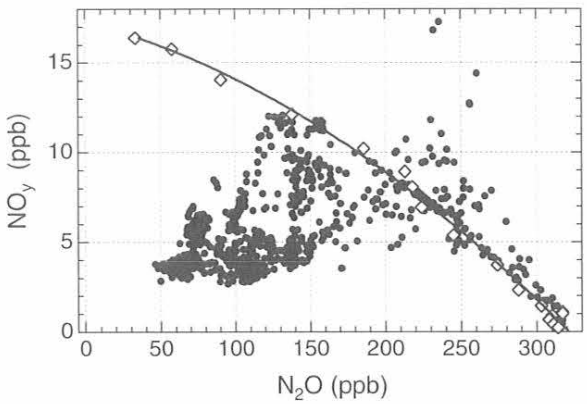

Fig. 5.25. Coincident in situ measurements of NO_y with the NOAA Aeronomy Laboratory total reactive nitrogen instrument [*Fahey et al.*, 1989] and N_2O with ACATS-IV on board the ER-2 aircraft during SOLVE (black circles). These data document severe and extensive denitrification in the Arctic vortex. The reference curve, a quadratic fit to NO_y and N_2O measured by the balloonborne MkIV interferometer on December 3, 1999 (open diamonds), represents the early-vortex NO_y:N_2O relationship before the onset of denitrification. Points below the reference curve indicate that air masses between 17 and 21 km altitude were denitrified by up to 75%. Nitrification at lower altitudes (14-16 km) is shown by points above the reference curve. (Figure adapted from *Popp et al.* [2001].)

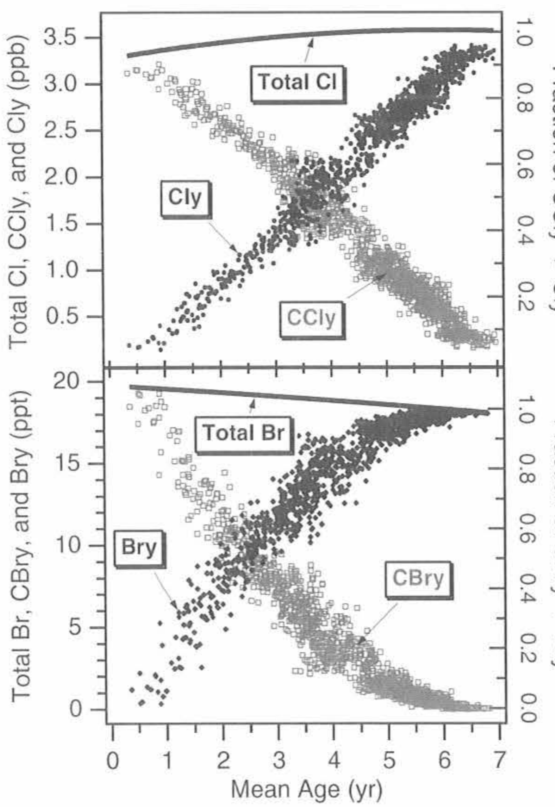

Fig. 5.24. Top: Total chlorine (solid curve), organic chlorine (CCl_y, gray squares), and inorganic chlorine (Cl_y, black circles) as a function of mean age for air masses sampled by ACATS-IV during SOLVE. The fraction of organic chlorine converted to inorganic chlorine reservoirs was approximated by the black circles using the right axis scale. Bottom: Same as the top graph, but for bromine. CCl_y and CBr_y are the sums of chlorinated and brominated source gases measured in the lower stratosphere by ACATS and the NCAR whole air sampler. Total chlorine and total bromine were determined from CMDL global surface trends of source gases with appropriate age spectral weightings. Cl_y and Br_y were calculated as the difference between total Cl (Br) and CCl_y (CBr_y). Mean ages were calculated from ACATS measurements of SF_6 in the lower stratosphere and the SF_6 global surface trend [*Geller et al.*, 1997].

column reduction of 117 ± 14 Dobson units (DUs) by late March 2000. *Salawitch et al.* [2002] studied the evolution of O_3:N_2O relationships to conclude that chemical O_3 loss between 14 and 22 km caused a 61-DU reduction of column O_3 between late November 1999 and March 5, 2000. The ozone loss and loss rates deduced in these three studies are in good agreement.

Grooss et al. [2002] used data from ACATS-IV and other instruments to initialize a stratospheric chemistry and transport model, the Chemical Lagrangian Model of the Stratosphere (CLaMS), that simulated Arctic ozone loss during SOLVE. Model simulations agreed well with the observed ozone loss at 450 K (about 19-km altitude) but tended to underestimate O_3 losses at higher altitudes, probably because of the limited amount of data used to initialize the model at higher altitudes and the absence of diabatic descent in the model.

Accurate differentiation between wintertime changes in vortex O_3 caused by chemistry and those caused by transport relies strongly on determinations of how much extra-vortex air mixes into the vortex. The vortex edge is a barrier to the exchange of midlatitude and vortex air. Previous work implied that differences between vortex and extra-vortex tracer-tracer relationships were due to large-scale, homogeneous descent in the vortex and significant in-mixing of extra-vortex air [*Plumb et al.*, 2000]. Descent can be roughly estimated by tracking the motion of air parcels with an inert tracer, as shown for N_2O in Figure 5.27. Most of the molecules measured by ACATS-IV and LACE are inert in the vortex, lacking local sources and

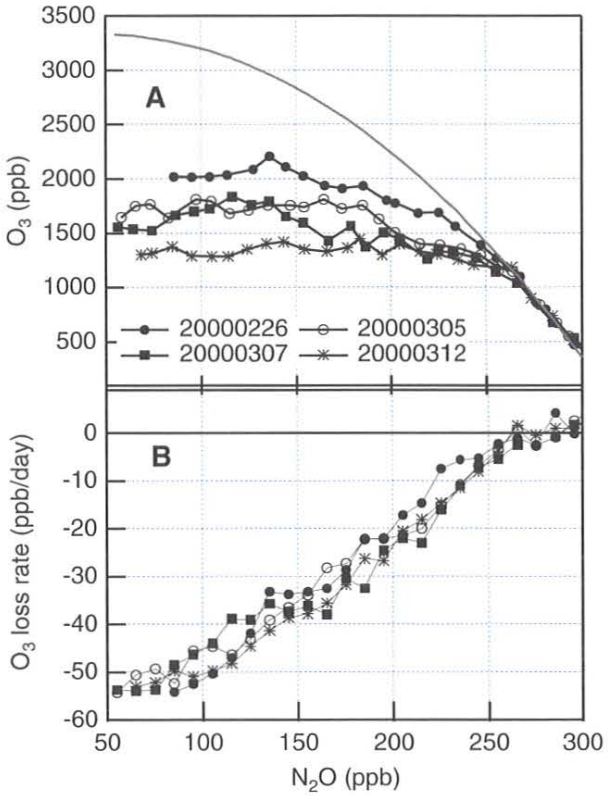

Fig. 5.26. (a) Coincident in situ measurements of O_3 with the NOAA Aeronomy Laboratory dual-beam ultraviolet photometer [*Proffitt and McLaughlin*, 1983] and N_2O with ACATS-IV on board the ER-2 aircraft during SOLVE. These data show the wintertime losses of O_3 in the Arctic vortex. The gray reference curve, a quadratic fit to O_3 and N_2O measured during four ER-2 and balloon flights between December 3, 1999, and February 3, 2000, represents the early-vortex O_3:N_2O relationship prior to ozone losses. Data from subsequent ER-2 flights demonstrate cumulative O_3 losses of up to 60% from early February to mid-March 2000. (b) Ozone loss rates calculated from differences between O_3:N_2O relationships in the early vortex and for the four ER-2 flights shown in (a). (Figure adapted from *Richard et al.* [2001].)

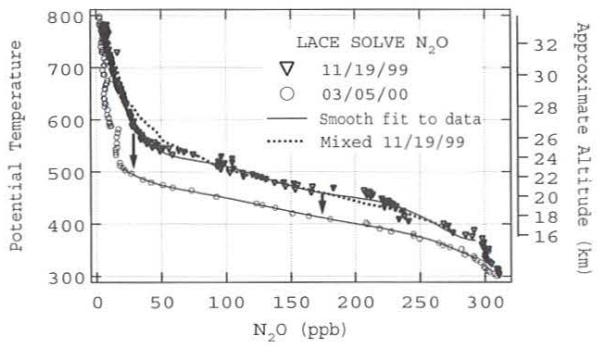

Fig. 5.27. Profiles of N_2O as a function of potential temperature (K) from LACE for the two OMS balloon flights during the SOLVE mission. Solid curves through the data are fits used in the calculation of descent in the vortex between the flights. Also included is a representation of a well-mixed early-vortex profile (dashed curve) from the differential descent mixing calculation.

sinks on the time scales of transport. Because these molecules have different vertical mixing ratio profiles, each molecule allows for an independent measurement of descent and other transport characteristics. This calculation of descent is only valid if mixing between air parcels of differing tracer concentration does not occur on similar time scales. In the absence of chemistry, this type of mixing can be seen as a shift in the curved tracer-tracer correlation plots (Figure 5.28).

Ray et al. [2002] were unable to produce the vortex tracer-tracer relationships observed by LACE and ACATS-IV during SOLVE by modeling homogeneous descent and in-mixing of extra-vortex air. They showed, instead, that differential descent and isentropic mixing within the vortex could produce the observed vortex relationships. These processes were folded into the descent calculations (dotted line in Figure 5.27) to give the final descent rates shown in Figure 5.29a. Note the good agreement across all tracers. The differential descent needed to reproduce the changes in tracer-tracer correlations is shown in Figure 5.29b. The lack of significant in-mixing of extra-vortex air during winter 1999/2000 is an important finding because it identifies chemistry, not transport, as the predominant cause of the large ozone losses observed during SOLVE. Analyses

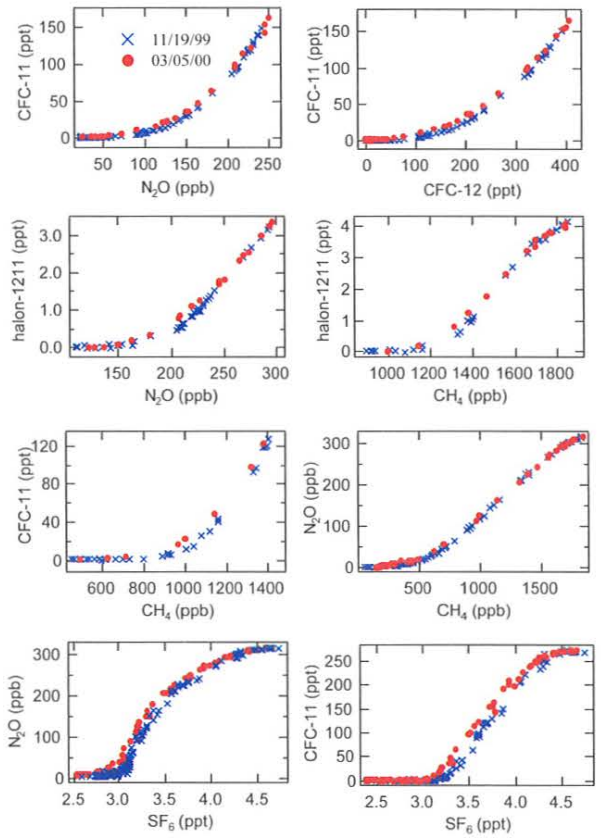

Fig. 5.28. Tracer-tracer correlation curves from the two LACE SOLVE flights. Data from the second flight are significantly shifted from the first flight toward the concave side of the curves, which suggests mixing of some type occurred.

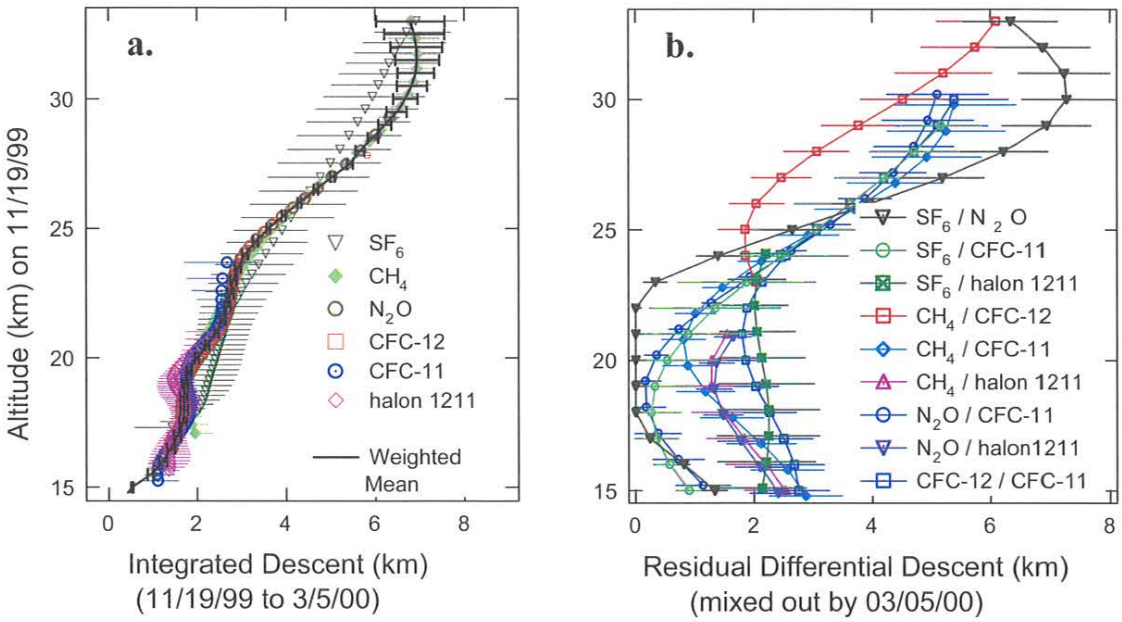

Fig. 5.29. (a) Integrated and (b) differential descent deduced from measurements associated with two LACE flights within the core of the Arctic vortex during SOLVE. Error bars represent the calculated statistical uncertainty.

by *Greenblatt et al.* [2002] and *Morgenstern et al.* [2002] using unified N_2O and ACATS-IV tracer data also conclude that the 1999/2000 Arctic vortex was strongly isolated and experienced little in-mixing.

The importance of accurate determinations of mean age distributions in the stratosphere has been stressed by *Andrews et al.* [2001]. Compared with mean ages calculated from in situ measurements of age tracers like SF_6 and CO_2, mean ages from many stratospheric transport models are underestimated by as much as a factor of 2. If general circulation rates in the models are decreased to increase mean ages, model tracer distributions fail to match observed distributions. Hence, model evaluations of important environmental issues related to trace gases, such as the impacts of exhaust from a proposed fleet of stratospheric aircraft and ozone layer recovery time scales, may be of limited accuracy until these discrepancies between models and observations are reduced. Using long-lived tracer data from ACATS, LACE, and other instruments, *Andrews et al.* [2002] have constructed accurate distributions of mean age in the stratosphere that will help improve the transport in models.

SF_6 is a strong greenhouse gas with a long lifetime. Estimating its atmospheric lifetime is important in terms of its contribution to the Earth's radiative budget as well as its use as a tracer of atmospheric motion. The stratospheric lifetime of SF_6 is dominated by loss that occurs in the mesosphere. Evidence of this loss is measurable in mesospheric air that descends into the polar vortices. Moore et al. [Measured SF_6 loss and its influence on age-of-air calculations, in preparation, 2002] calculated the stratospheric lifetime of SF_6 from OMS data assuming that (a) the age of air calculated with CO_2 data [*Andrews et al.*, 2002] is correct, and differences between CO_2 and SF_6 age-of-air estimates from vortex data (Figure 5.30) are due to SF_6 loss, and (b) the loss of SF_6 occurs over 6 months, and the mesospheric air descends only into the northern vortex (6 months later the process repeats into the southern

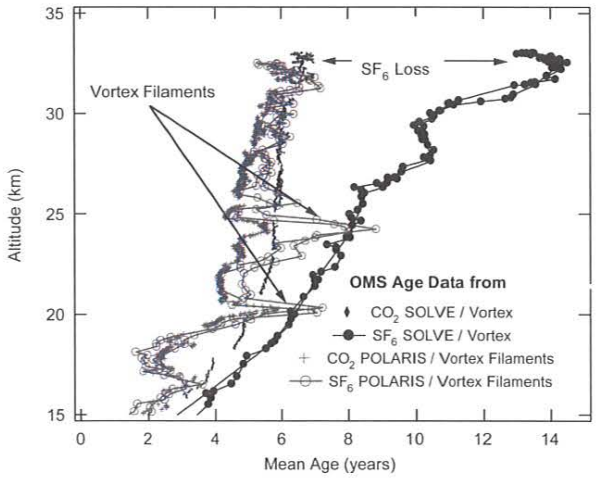

Fig. 5.30. Age-of-air estimates from both CO_2 and SF_6 data, assuming all stratospheric sources or sinks are taken into account. The difference between these two age estimates, seen both in the vortex filaments and the vortex core data, is then assumed to be due to SF_6 loss in the mesosphere.

vortex). The net loss within the northern vortex was multiplied by two to estimate the yearly loss rate. Their new estimate for the stratospheric lifetime of SF_6 is 600 (+200, −100) years, which is better constrained than the previously reported range of 600-3200 years [*Morris et al.*, 1995]. The upper bound in the new estimate is less certain than the lower bound because of an uncertainty in SF_6 loss above 32 km within the vortex.

Significant global O_3 destruction will continue well into the 21st century because of the high halogen burden of the stratosphere [*Prinn et al.*, 1999]. Accurate predictions of future O_3 levels require accurate determinations of halogen budgets and their trends. Stratospheric chlorine [*Woodbridge et al.*, 1995] and bromine [*Wamsley et al.*, 1998] budgets are periodically calculated from ACATS, LACE, and WAS measurements of halogenated source gases, allowing the determination of trends. The calculation methods have been revised over time to reflect significant changes in the tropospheric trends of some halocarbons. An important, recent refinement in these calculations is the weighting of tropospheric trends with age spectra [*Hall and Plumb*, 1994; *Andrews et al.*, 2001] instead of mean age, to determine trends in total chlorine (Cl_{tot}) and total bromine (Br_{tot}) entering the stratosphere [*Elkins*, 2000]. These revisions improve calculations of total inorganic chlorine (Cl_y) and total inorganic bromine (Br_y) as the difference between total chlorine (bromine) and the sum of chlorinated (brominated) source gases CCl_y (CBr_y).

Schauffler et al. [2002] have recently revised the stratospheric chlorine budget based on WAS and ACATS-IV measurements made during SOLVE. A comparison of ACATS-IV and WAS CCl_y for SOLVE reveals differences of 0.015-0.190 ppb (Figure 5.31), with WAS values always larger because the ACATS-IV method does not account for chlorine from CFC-114, CFC-114a, CFC-115, CH_2Cl_2, C_2Cl_4, HCFC-142b, and HCFC-141b. These omissions account for 0.023-0.130 ppb of the CCl_y differences. The rest of the discrepancy results from calibration-scale differences and disparity in the HCFC-22 and CH_3Cl mixing ratios calculated by ACATS-IV but measured by WAS. The two independent data sets are complementary in that ACATS reports CCl_y more frequently (every 140 seconds) than WAS, but the WAS CCl_y data are inherently more accurate.

Trends in Cl_y determined from ACATS and LACE measurements near 19-, 20.5-, and 27.5-km altitude over the period 1992-2000 imply that Cl_y either peaked or leveled off by the year 2000 (Figure 5.32a). The sum of chlorinated source gases (CCl_y, or ETCl) measured at the surface by CMDL (Figure 5.32a) illustrates the decreasing trend in Cl_{tot} [*Montzka et al.*, 1999], largely because of the rapid decline in CH_3CCl_3. These surface CCl_y data represent an upper limit for Cl_y and are closely matched by Halogen Occultation Experiment (HALOE) Cl_y (HCl) data at 55-km altitude, where near-complete conversion of CCl_y to Cl_y has occurred (Figure 5.32a). Upward trends in Br_y, apparent at all three altitudes (Figure 5.32b), are driven predominantly by continued emissions of halons. The increasing sum of brominated source gases (CBr_y) measured at the surface by CMDL provides an upper limit for Br_y.

Of pivotal importance to stratospheric ozone are the combined influences of chlorine and bromine trends. The

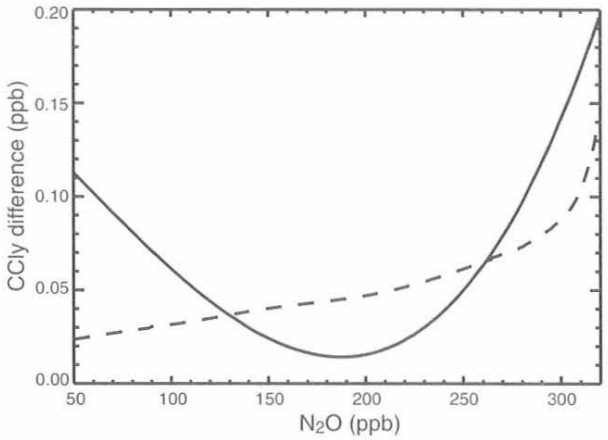

Fig. 5.31. Differences between WAS and ACATS-IV determinations of CCl_y as a function of N_2O (solid curve). Values range from 0.015 to 0.190 ppb. Partial differences in CCl_y that result from the ACATS omission of CFC-114, CFC-114a, CFC-115, CH_2Cl_2, C_2Cl_4, HCFC-142b, and HCFC-141b (dashed curve) range from 0.023 to 0.130 ppb. The remaining differences between WAS and ACATS-IV CCl_y result from calibration scale differences and the fact that CH_3Cl and HCFC-22 are calculated by ACATS-IV and measured by WAS. (Figure adapted from *Schauffler et al.* [2002].)

weighted sum of inorganic chlorine and bromine, namely equivalent inorganic chlorine ($ECl_y = Cl_y + 45 \times Br_y$), reflects the fact that Br_y is on average 45 times more efficient than Cl_y at the destruction of O_3 [*Daniel et al.*, 1999]. Trends in ECl_y (Figure 5.32c) mimic the decline or leveling off of Cl_y (Figure 5.32a), because Cl_y is 100-150 times more abundant than Br_y and the upward Br_y trend does little to offset the decreasing trend in Cl_y. Future trends in ECl_y, and hence O_3, are strongly dependent on this interplay between increasing bromine and decreasing chlorine abundance. Continued halon accumulation in the atmosphere may eventually overshadow reduced chlorine burdens, especially as the rate of CH_3CCl_3 decline approaches zero.

Up to this point, HATS airborne GCs were specifically designed to make measurements in the upper troposphere and lower stratosphere. Tropospheric issues such as air quality and the accumulation of greenhouse gases are expected to take a higher priority in this century. Funding was provided by the NASA Instrument Incubator Program to develop the PAN and other Trace Hydrohalocarbons Experiment (PANTHER) next-generation airborne GC. A mass selective detector will be combined with two or more ECD channels to focus on more reactive and shorter-lived species. The first test flight of PANTHER is scheduled for spring 2002 on the NASA ER-2 aircraft. Key molecules measured on this test flight will include peroxyacetyl nitrate (PAN), acetone ($CH_3C(O)CH_3$), and HCFCs. PAN comprises the largest fraction of oxides of nitrogen (NO_y) under natural conditions in the troposphere and is a precursor of O_3. Acetone is a precursor of PAN and an important source of hydroxyl radical in the upper troposphere.

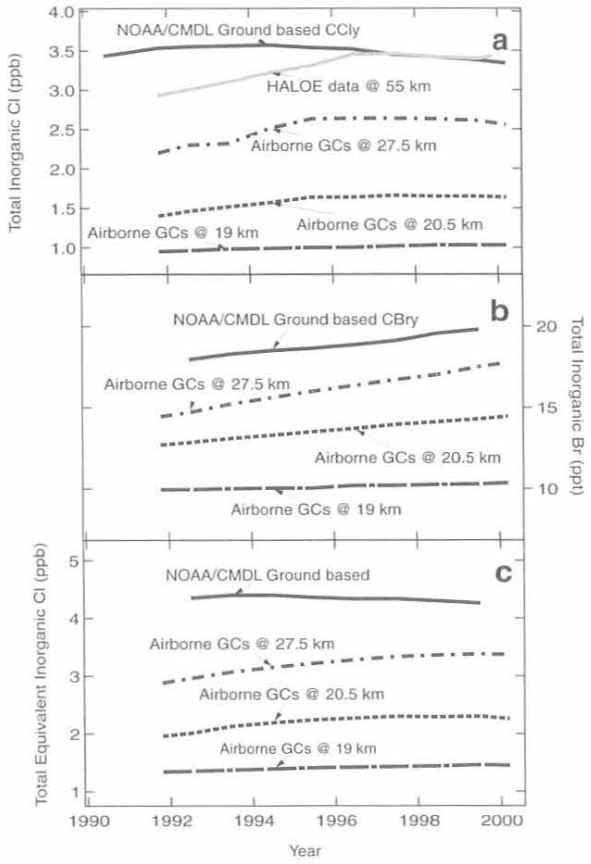

Fig. 5.32. Estimates of total inorganic halogen from airborne GCs (including ACATS and LACE): (a) total inorganic chlorine (ppb), (b) total inorganic bromine (ppt), and (c) total equivalent inorganic chlorine (ppb), at equivalent altitudes of 19, 20.5, and 27.5 km. HALOE inorganic chlorine data at 55 km are plotted in (a) (updated by *Anderson et al.* [2000]). CMDL ground-based data are plotted in (a)-(c).

5.4. Ocean Projects

5.4.1. Data Analysis

Natural halocarbons are important contributors to the destruction of stratospheric ozone. For example, methyl bromide (CH_3Br) and methyl chloride (CH_3Cl) together are the source of about one-quarter of the equivalent chlorine in the troposphere [*Butler*, 2000], where equivalent chlorine is one way to evaluate the ozone-depleting capacity of the atmosphere [*Daniel et al.*, 1995]. Other brominated compounds, such as dibromomethane (CH_2Br_2) and bromoform ($CHBr_3$), also might be significant sources of bromine to the upper atmosphere [e.g., *Schauffler et al.*, 1999; *Sturges et al.*, 2000]. An understanding of the sources and sinks of these compounds would enable the prediction of changes in the cycling of these compounds associated with climate change. Because the oceans are both a source and a sink of most natural halocarbons, oceanic measurements have constituted one component of the HATS group research effort.

Data obtained from previous field missions were analyzed during 2000-2001. The variability in sea surface temperature (SST) has been shown to account for one-half to two-thirds of the variability in methyl bromide oceanic saturations, according to *King et al.* [2000]. In that study, data from six cruises were fitted with two quadratic equations. While global extrapolations with this relationship appear reasonable, this relationship does not accurately reproduce observations on a regional basis. However, reexamination of the data, along with inclusion of data from a 1999 expedition to the Pacific Ocean, has significantly improved the ability to reproduce field observations.

Data from seven research cruises (five conducted by CMDL and two by Dalhousie University) were divided seasonally into two data sets: spring-summer and fall-winter. These data include measurements from the Atlantic [*Lobert et al.*, 1996; *Groszko and Moore*, 1998; *King et al.*, 2000], the Pacific [*Lobert et al.*, 1995; *Groszko and Moore*, 1998; *King et al.*, 2000; unpublished CMDL data], and the Southern Ocean [*Lobert et al.*, 1997]. Measurements made between March 20 and September 21 were considered spring-summer if north of the equator and fall-winter if south of the equator. Data collected during the remainder of the year were assigned to fall-winter if north of the equator and spring-summer if south of the equator. Each seasonal data set was fitted with two quadratic equations, describing data above and below 16°C (Figure 5.33).

The new equations represent a significant improvement over the existing equations, particularly in temperate regions. For example, the previous equations could account for only about 15% of the seasonal difference (summertime supersaturations and fall undersaturations) in CH_3Br saturation anomaly observed in the North Atlantic temperate waters [*King et al.*, 2000]. However, the new equations can reasonably reproduce the observed seasonal difference for CH_3Br in these waters. The seasonal SST relationships also improve the ability to estimate the mean saturation anomaly for a given data set. For the two most recent cruises, Gas Exchange Experiment (Gas Ex 98) [*King et al.*, 2000] and Bromine Air-sea Cruise Pacific (BACPAC 99) [*Schnell et al.*, 2001], the mean CH_3Br saturation anomalies estimated with the new equations are about 90% of the measured values. In contrast, the mean saturation anomalies as determined with the old equations [*King et al.*, 2000] are only about 60% of the measured values.

Methyl bromide saturation anomaly maps have been generated with the seasonal SST relationships and a global map of SSTs (Figure 5.34). The SST data set consists of 1° × 1° monthly means from the National Oceanographic Data Center (NODC) [*Levitus*, 1982]. Each grid point represents a 3-mo average value. In this model CH_3Br undersaturations are predicted in both the tropics and polar regions throughout the year. The temperate waters, however, show a strong seasonal cycle in both hemispheres. With the data used to create these maps, the global, annually averaged CH_3Br saturation anomaly is calculated

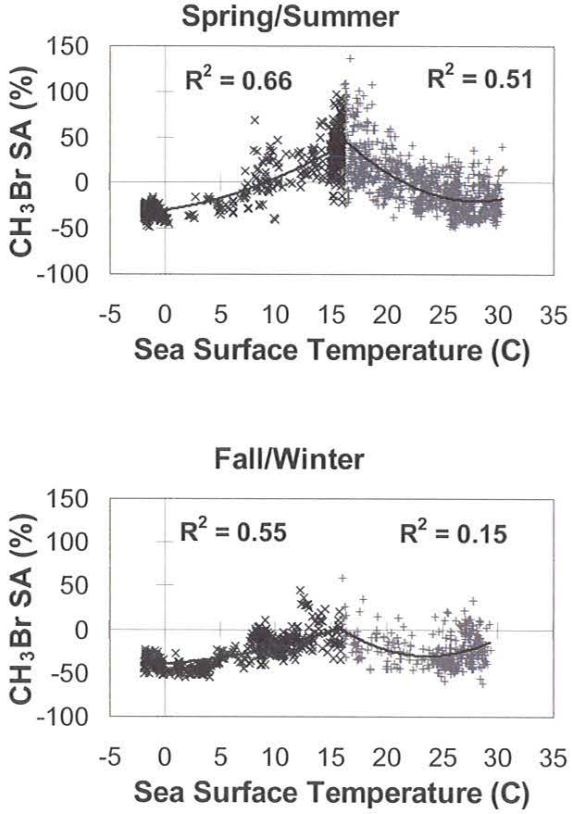

Fig. 5.33. Methyl bromide saturation anomaly data from five CMDL cruises and two Dalhousie University cruises between 1994 and 1999, plotted as a function of sea surface temperature. The data are divided seasonally, with local spring and summer data in the upper plot and local fall and winter data in the lower plot. Quadratic fits are used to describe data above and below 16°C for each seasonal data set.

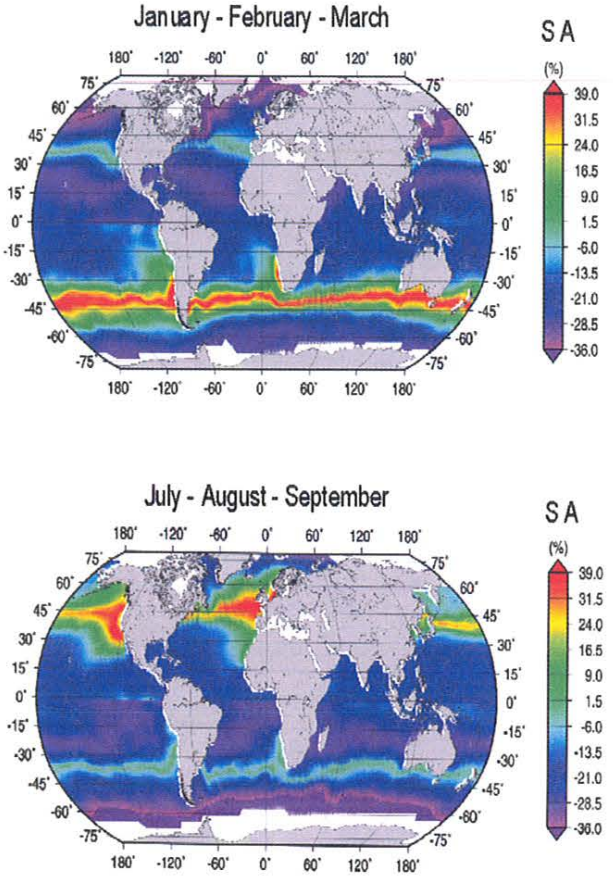

Fig. 5.34. Methyl bromide saturation anomalies plotted as 3-mo averages on 1° by 1° grid size. These maps were generated with relationships between saturation anomaly and sea surface temperature (shown in Figure 5.33). White spaces represent regions with insufficient sea surface temperature data to calculate a value for the CH_3Br saturation anomaly.

to be −15.5%. The calculated global, annually averaged CH_3Br flux is −19.9 Gg yr^{-1}. Both of these values agree with other published estimates [e.g., *Lobert et al.*, 1997; *King et al.*, 2000].

5.4.2. 2001 Ocean Cruise

During fall 2001 the HATS group participated on a research cruise in the Southern Ocean. The Australian ship *Aurora Australis* departed Hobart, Tasmania, on October 29 and returned to Hobart on December 13. The vessel headed south toward the Antarctic coast before returning to Australia, retracing a previous Climate Variability and Predictability (CLIVAR) cruise track (Figure 5.35). The HATS group measured over 20 halogenated compounds in the surface seawater and overlying atmosphere. The results will be coordinated with those obtained by research groups from NOAA Atlantic Oceanographic and Meteorological Laboratory (AOML) (halocarbon depth profiles) and the University of California at Irvine (methyl bromide and methyl chloride degradation rates).

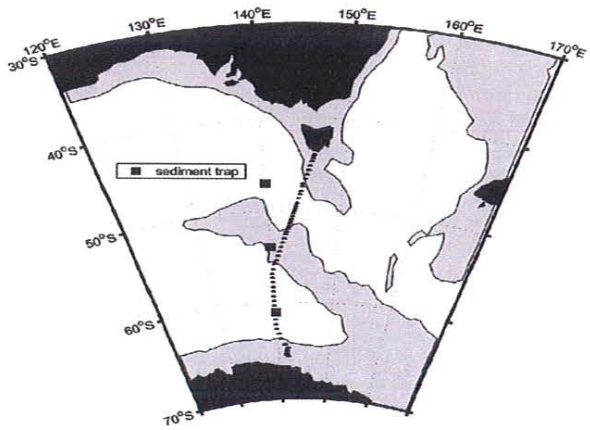

Fig. 5.35. The cruise track for the fall 2001 cruise on which the HATS group participated. The *Aurora Australis* departed Hobart, Tasmania, and returned to Hobart after approaching the Antarctic coast.

5.5. Special Projects

5.5.1. Methyl Halide Emissions from Tomato Plants

Fieldwork

The atmospheric budgets of most natural halocarbons are poorly defined. For both methyl bromide (CH_3Br) and methyl chloride (CH_3Cl), best estimates of the known sinks outweigh best estimates of the known sources by 30-50% [*Kurylo et al.*, 1999]. Although plant production of natural halocarbons has not been studied extensively, there is considerable new evidence that plants are involved in the cycling of these compounds. Previous studies have primarily involved the use of a flux chamber, which does not isolate the plant from the soil and potentially stresses the plant [e.g., *Gan et al.*, 1998; *Redeker et al.*, 2000; *Rhew et al.*, 2000, 2001]. Soils are potentially problematic because they have been observed to remove CH_3Br from the atmosphere [e.g., *Varner et al.*, 1999].

The HATS group conducted an experiment in a hydroponic greenhouse in Northern California (McKinleyville) over a 2-wk period in July 2001. The greenhouse was covered with double-layered polyethylene and housed about 400 tomato plants (*Lycopersicon esculentum)*. The plants were grown in bags of inert support material (Pearlite) without soil and were flushed with an aqueous nutrient mixture at frequent intervals throughout the day. During each experiment, the greenhouse was sealed, and halocarbon concentrations were measured in the greenhouse atmosphere with a GC-MSD located at the site. Sampling lines were placed in the center and at one end of the greenhouse. Fans were used to keep the greenhouse atmosphere well mixed. No concentration differences were observed between the two sampling locations. Experiments were started in the late afternoon/early evening and were run until the air temperature in the greenhouse exceeded about 35°C, usually about noon the following day. Eight experiments were run in total, and each experiment lasted 16-20 hours. The standard nutrient mixture was used first for two control experiments (C-1 and C-2). This nutrient mixture contained no significant halide concentrations. A solution containing about 5 ppm Br^-, Cl^-, and I^- was added in line with the nutrient mixture during the third, fourth, and fifth experiments (H5-1, H5-2, and H5-3). During the final three experiments (H20-1, H20-2, and H20-3), a solution of about 20 ppm Br^-, Cl^-, and I^- was added in line with the nutrient mixture. These halide solutions were added continuously over the course of several days, not just during the experiments themselves.

Results and Discussion

During C-1 and C-2, no production of CH_3Br (Figure 5.36a) or CH_3Cl was observed, but methyl iodide (CH_3I) (Figure 5.36b) increased by a factor of about 5 by the end of the experiments. Production was also observed for several other halogenated compounds, including bromochloromethane (CH_2BrCl), dibromomethane (CH_2Br_2), dibromochloromethane ($CHBr_2Cl$), and bromoform ($CHBr_3$) (Figure 5.36c). In general, anthropogenic compounds, such as CFC-11 (Figure 5.36d), CFC-113, and halon-1211, remained relatively constant over the course of the study, suggesting that large-scale contamination from materials in the greenhouse or from the greenhouse itself was unlikely.

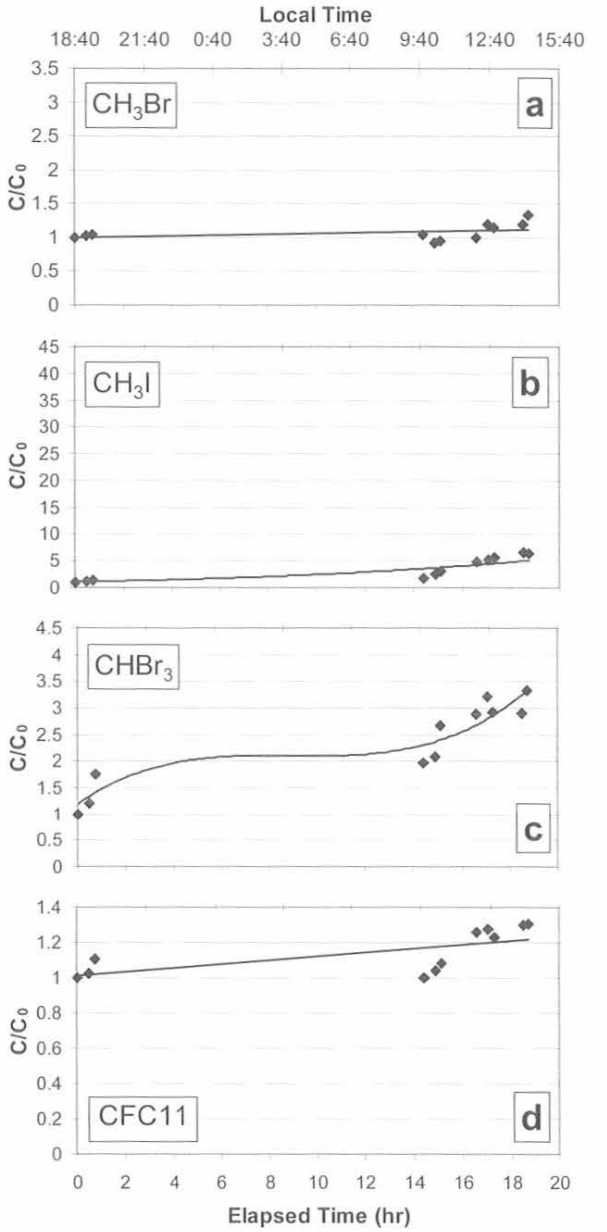

Fig. 5.36. Concentration changes of (a) CH_3Br, (b) CH_3I, (c) $CHBr_3$, and (d) CFC-11, during a greenhouse experiment, plotted as a function of time. All concentrations were normalized to the corresponding initial concentration (C/C_0). During this experiment, no halide ions were added to the nutrient mixture.

The addition of the halide solution affected the production rates of only CH_3Br and CH_3I (Figure 5.37a,b).

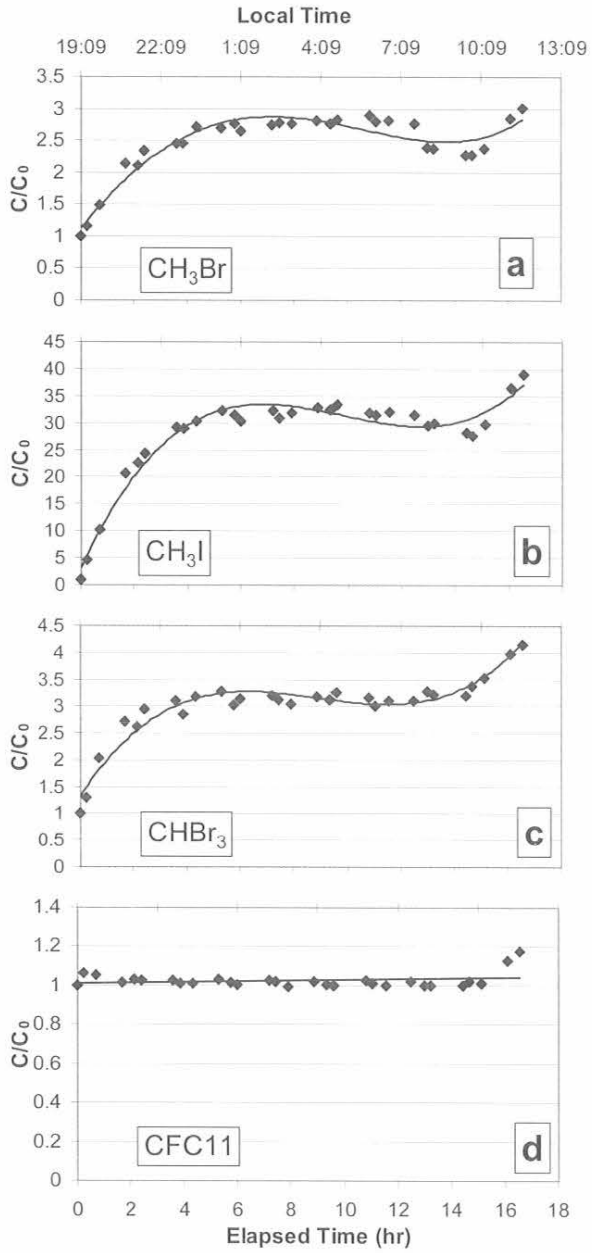

Fig. 5.37. Concentration changes of (a) CH_3Br, (b) CH_3I, (c) $CHBr_3$, and (d) CFC-11, during a greenhouse experiment, plotted as a function of time. All concentrations were normalized to the corresponding initial concentration (C/C_0). During this experiment, a solution containing about 20 ppm Br^-, Cl^-, and I^- flushed the plants with the nutrient mixture.

During experiments H20-1, H20-2, and H20-3, CH_3Br increased by nearly a factor of 3. Production of CH_3I increased by a factor of about 35 during these experiments, almost an order of magnitude more than with the standard nutrient mixture alone. Production for other halogenated compounds, such as $CHBr_3$ (Figure 5.37c) and $CHBr_2Cl$, did not change noticeably between experiments run with and without the halide solution.

Similar results were observed for the H5 experiments. Only CH_3Br and CH_3I production differed from the other experiments. The production for those two compounds increased with each experiment. Production during H5-3 approached the values that were observed during the H20 experiments. This suggests that production of CH_3Br and CH_3I by tomato plants is a function of halide concentration. More studies are necessary to determine if these observations are reproducible for these and other plants.

Although tomato plants were chosen for little other reason than opportunity, this study suggests that many plants could emit significant amounts of organic halogens to the atmosphere. It also supports propositions from other investigators that there is a relationship between halide concentration in the soil and organic halogen production by plants [e.g., *Redeker et al.*, 2000; *Rhew et al.*, 2000]. This preliminary study has raised many questions. One question concerns the production of polybrominated compounds when no halides were added, whereas CH_3Br concentrations remained constant. It is also unknown why the production of CH_3Br and CH_3I increased with the addition of the halide solution while that of other halocarbons did not. The potential variability of production rates as a function of plant growth stage was also not addressed in this study. Further studies of these and other plants will be necessary before these questions can be adequately addressed.

5.5.2. Trans-Siberian Observations into the Chemistry of the Atmosphere (TROICA)

From June 27 to July 10, 2001, about 11,000 in situ measurements of CFC-12, halon-1211, N_2O, and SF_6, and nearly 5000 measurements of CFC-11, CFC-113, $CHCl_3$, CH_3CCl_3, CCl_4, CH_4, and H_2 were made along 17,000 km of the fully electrified trans-Siberian railway between Moscow and Khabarovsk, Russia (Figure 5.38), with the ACATS-IV gas chromatograph (GC). These measurements were part of the seventh Trans-Siberian Observations into the Chemistry of the Atmosphere (TROICA-7) scientific expedition, a collaboration between CMDL, the Coooperative Institute for Research in Environmental Sciences (CIRES), NASA, the Max Planck Institute for Chemistry (Mainz, Germany), and the Russian Institute of Atmospheric Physics (Moscow). TROICA expeditions were inaugurated by German and Russian scientists in 1995 and have taken place annually during different seasons [*Crutzen et al.*, 1998; *Oberlander et al.*, 2002]. The primary CMDL objective for TROICA-7 was to make frequent (every 70 or 140 seconds) measurements of halocarbon and greenhouse gases along the trans-Siberian railway, creating a database to which future TROICA measurements of these gases can be compared. CMDL participation in TROICA-7 produced the first extensive set of halocarbon measurements in Russia by American scientists.

As during past TROICA expeditions, German and Russian scientists operated in situ analyzers for CO, CO_2, O_3, CH_4, NO_x, ^{222}Rn, H_2O, aerosols, solar radiation, temperature, pressure, and relative humidity [*Crutzen et al.*, 1998]. A global positioning system receiver tracked

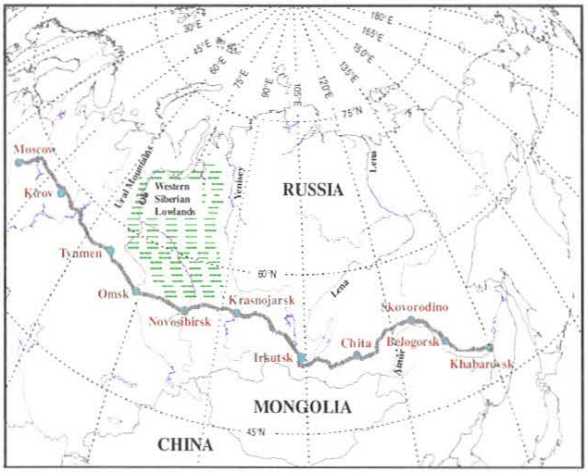

Fig. 5.38. Route of the TROICA-7 science expedition along the trans-Siberian railway. Each of the transects, Moscow-Khabarovsk and Khabarovsk-Moscow, was approximately 8500 km in length and took 6.25 days. Major cities along the railway are indicated by filled circles.

movements of the train, and visual observations along the route were recorded in detail. A microwave temperature profiler was also part of the payload. All instruments were housed in a special rail car (Research Institute of Railroad Transport of Russia) situated immediately behind the electric locomotive. Air intakes for instruments were attached to a frame structure on top of the science car. ACATS-IV sampled air at approximately 4 L min^{-1} through 5 m of 6.4-mm-outside-diameter Dekabon tubing with a Teflon diaphragm pump (model UN05, KNF Neuberger Inc., Princeton, New Jersey). A 2-mm-pore glass fiber filter was used to keep large particles out of the intake tubing. The sample stream was dried with $Mg(ClO_4)_2$.

The train traveled at a mean and maximum speed of 57 and 129 km h^{-1}. Numerous stops were made during the 6.25 days required to travel each direction. There were 216 scheduled stops at stations with durations of 2-90 minutes. Track maintenance and stop signals accounted for 43 unscheduled, non-station stops with durations of 1-69 minutes. In general, population density decreased with distance from Moscow, though large, industrialized cities were encountered almost daily along the length of the railway. East of the Ural Mountains, the population density is greatest in southern Siberia, near the railway. Rural areas were typically birch and larch forest (taiga) or rolling grasslands with some large lowland areas. The Moscow-Khabarovsk segment of the railway spans latitudes of 48.6° to 58.6°N and altitudes of 0 to 998 m above sea level. Temperature ranged from 3° to 33°C, with three daytime highs >30°C and three nighttime lows <10°C. Rain, heavy at times, was encountered on 12 of the 14 travel days.

Large fluctuations in the mixing ratios of some gases were observed during the expedition, as illustrated by the time series for the refrigerant CFC-12 and fire extinguishing agent halon-1211 (Figure 5.39). The variability (1 standard

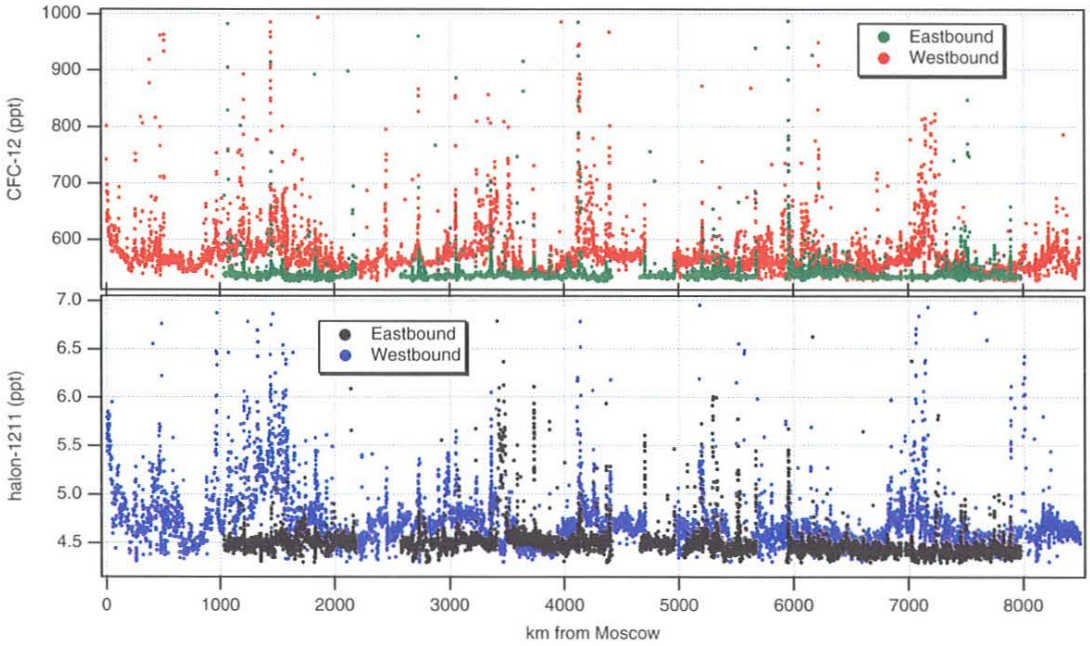

Fig. 5.39. Time series of CFC-12 (top) and halon-1211 (bottom) mixing ratios during TROICA-7 as a function of distance from Moscow. For CFC-12, there were 34 and 83 measurements >1000 ppt during the eastbound and westbound transects, respectively, that are off-scale in this figure. There were 2 eastbound and 41 westbound halon-1211 measurements >7 ppt that are off-scale. Of interest for these two gases are their high variability along the railway and their generally higher mixing ratios during the westbound transect.

deviation) of every gas measured along the railway was at least 50% greater than its measurement precision (Table 5.8). Variability relative to the mean mixing ratio was very high (>70%) for $CHCl_3$ and CO; 11-32% for CFC-12, halon-1211, H_2, and CO_2; 6-9% for CFC-113 and CH_4; and <3% for N_2O, SF_6, CFC-11, CH_3CCl_3, and CCl_4. Fluctuations in mixing ratio observed along the railway were also much greater than at Point Barrow, Alaska (BRW), during June-July 2001 (Table 5.8) except for CH_3CCl_3, which showed about the same low variability at both locations. Ratios of TROICA-7 to BRW variability for gases other than CH_3CCl_3 ranged from 1.7 for SF_6 to 59 for CFC-12.

For gases that exhibited concentrations higher than the northern hemispheric background, a major concern is the possibility of air sample contamination due to train-based sources forward and/or aft of the sampling inlets. No known sources of the measured gases were located forward of the sample inlets, but >100 m aft there were small coal-fired water heaters in passenger carriages and a working air conditioner in the restaurant car. There was also an inoperative air conditioning unit in the science carriage with no discernible pressure of CFC-12. Intuitively, a forward source would frequently contaminate the air stream sampled by instruments, especially at high train speeds. An aft source could have contaminated samples when the train was moving slowly or stopped.

To explore the possibility of contamination by train-based sources, data for four highly variable gases (CFC-12, halon-1211, CO, and CO_2) were separated by train speed: high, low, and stopped. Forward contamination of samples was investigated by comparison of data at high train speeds with CMDL data at remote, high-latitude northern hemisphere sites during June-July 2001. For these gases, 30-60% of the data taken at high train speeds were representative of well-mixed, background air masses, indicating that samples were not consistently contaminated by forward sources. This is supported by the fact that elevated mixing ratios (>80th percentile) were detected less frequently at high train speeds than when the train was stopped. However, this evidence, along with significantly lower fractions of background CFC-12 and CO mixing ratios at stops compared with high train speeds, suggests that aft sources on the train many have contaminated samples when the train was stopped. Of course, these biases may simply reflect the fact that the train stopped primarily at stations in populated areas where sources were present. To explore train contamination from aft sources during stops, CFC-12, halon-1211, CO, and CO_2 measurements made at scheduled station stops were separated from those made at unscheduled, non-station stops. For these four gases, fractions of background data at non-station stops (57-80%) were 1.4 to 2.3 times greater than at station stops (24-47%). Fractions of elevated mixing ratios at station stops were also factors of 1.3 to 3.5 higher than at non-station stops. Though these statistics for station and non-station stops do not preclude the possibility of sample contamination by the train during stops, they strongly imply that sources proximate to train stations in populated areas were responsible for the elevated mixing ratios measured during stops.

CFC-12 and halon-1211 concentrations were quite variable during both the eastbound and westbound transects of TROICA-7 (Figure 5.39), but were generally higher throughout the westbound return to Moscow because of large, sustained concentration increases observed on some nights. These increases, also seen in CO_2, ^{222}Rn, and $CHCl_3$ data (Figures 5.40 and 5.41), occurred beneath nocturnal temperature inversions that were much stronger and prolonged during the westbound transect (Figures 5.40a and 5.41a). Increases in ^{222}Rn and CO_2 beneath the nighttime inversions were generally broad and well-correlated because

TABLE 5.8. Summary Statistics of Gas Measurements During TROICA-7 and at Barrow, Alaska

	TROICA-7							
Gas	N	Mean	Median	Precision*	Variability†	75th – 25th Percentile	95th – 5th Percentile	BRW Variability‡
N_2O (ppt)	10815	316.7	316.4	0.6	1.9	1.1	3.7	0.8
SF_6 (ppt)	11086	5.00	4.99	0.05	0.15	0.07	0.19	0.09
CFC-12 (ppt)	11132	573	551	4	118	36	123	2
Halon-1211 (ppt)	11125	4.66	4.55	0.04	0.52	0.25	0.94	0.04
CFC-11 (ppt)	4629	263.0	262.0	0.5	5.3	1.3	6.3	1.2
CFC-113 (ppt)	4573	82.3	81.9	0.3	7.2	0.9	2.3	0.7
$CHCl_3$ (ppt)	4929	16.3	14.1	0.2	12.6	4.2	15.3	1.7
CH_3CCl_3 (ppt)	4700	38.9	38.8	0.5	0.8	1.1	2.1	0.8
CCl_4 (ppt)	4690	102.7	102.5	0.4	2.5	0.6	2.3	0.4
H_2 (ppb)	4634	549	507	14	177	66	350	15
CO (ppb)	8241	146	126	10	102	59	218	5
CH_4 (ppb)	4459	1882	1852	16	109	83	212	21
CO_2 (ppm)	10706	379.3	365.3	1	41.8	24.9	127.8	1.4

*Precision is expressed as the standard deviation of residuals of ACATS-IV calibration measurements made during the expedition, where residuals are deviations of raw calibration data from smoothed, drift-corrected calibration data.

†TROICA-7 variability is expressed as 1 standard deviation.

‡ BRW variability is expressed as the standard deviation of residuals of hourly averages of in situ observations made at Point Barrow, Alaska (72° N), during June-July 2001. Residuals are deviations from smooth curve fits to the data that account for seasonal cycles and longer-term trends.

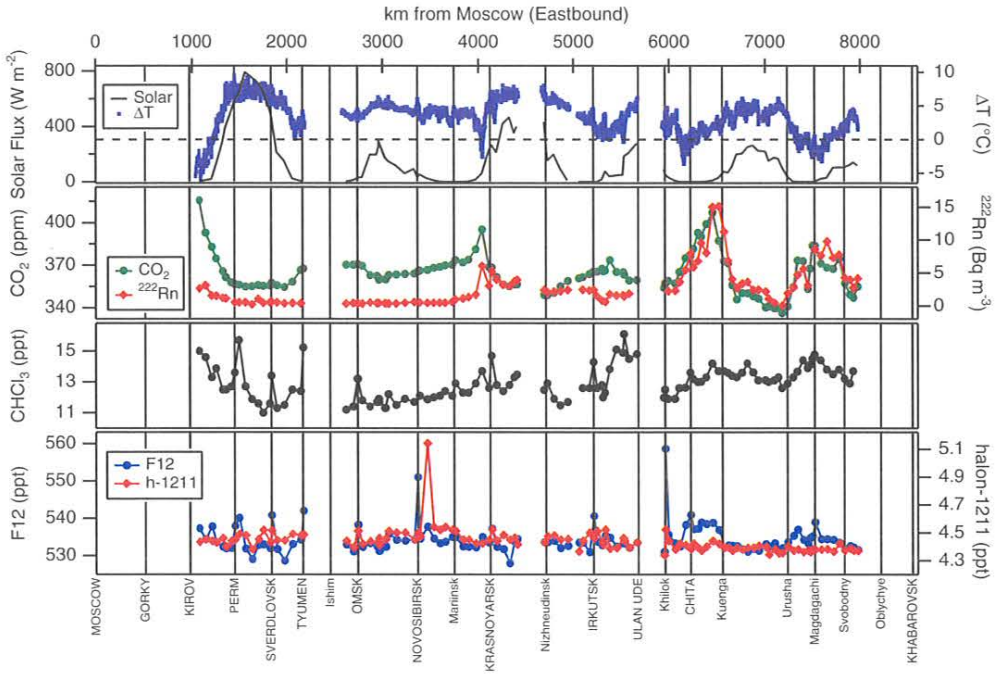

Fig. 5.40. Solar flux, temperature difference, and mixing ratios for CO_2, ^{222}Rn, CFC-12, halon-1211, and $CHCl_3$ during the eastbound transect of TROICA-7. The mixing ratios of these gases increased broadly beneath relatively weak temperature inversions during several nights of the transect. CFC-12, halon-1211, and $CHCl_3$ mixing ratios also sharply increased near several cities. Data for these gases are the 20th percentiles in 1-h windows. Solar fluxes identify daytime and nighttime periods. ΔT is the difference in temperature at 0 and 600 m above the science car roof such that $\Delta T < 0$ indicates a temperature inversion. Major cities along the railway are listed along the bottom axis.

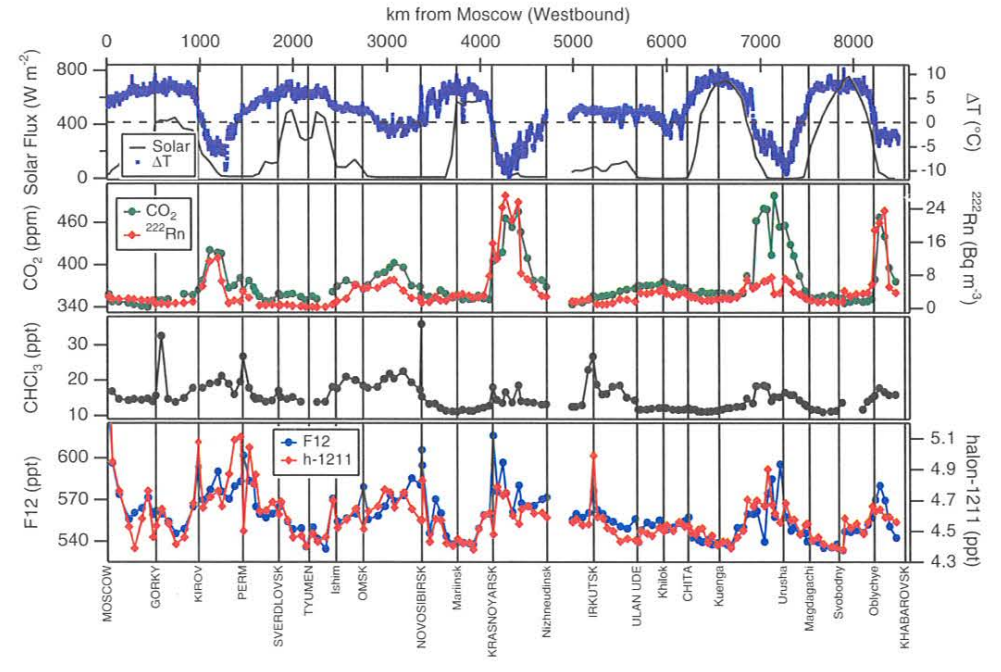

Fig. 5.41. Same as Figure 5.40, except for the westbound transect of TROICA-7. Time series should be viewed from right to left (east to west) as the train returned to Moscow. Several strong nighttime temperature inversions caused large, broad increases in gas concentrations. Note the greatly expanded concentration ranges compared with those in Figure 5.40, the result of stronger temperature inversions and perhaps greater emissions from upwind sources.

both gases are widely emitted by soils. Similar nighttime increases in ^{222}Rn, CO_2, and other gases have been observed during previous TROICA expeditions [*Bergamaschi et al.*, 1998; *Crutzen et al.*, 1998; *Oberlander et al.*, 2002]. $CHCl_3$, CFC-12, and halon-1211 mixing ratios increased broadly beneath several nighttime inversions and sharply near some cities. Nighttime increases in these halocarbons were typically coincident with increased ^{222}Rn and CO_2, but their magnitudes were not generally consistent with ^{222}Rn and CO_2 increases, possibly because of geographical variations in the strengths of halocarbon sources.

Analyses of the TROICA-7 data continue in an effort to characterize the source emissions, transport, and boundary layer dynamics responsible for the observed trace gas variability. Under the *Montreal Protocol on Substances that Deplete the Ozone Layer* [*UNEP*, 1987], non-Article 5 (developed) countries like Russia and the United States were required to cease production of halons and CFCs by January 1994 and 1996, respectively. Economic difficulties prevented Russia from meeting these target dates. Only with substantial financial incentives did Russia finally cease CFC and halon production in December 2000. Inspectors have since verified that Russia is no longer producing CFCs and halons. It is of great interest now to determine whether the detected emissions of CFC-12 and halon-1211 along the trans-Siberian railway are related to stockpile leaks, discharges from in-use structures and equipment, or seepage from abandoned structures and discarded equipment. CMDL scientists intend to be part of the next TROICA expedition proposed for winter 2002/2003.

5.5.3. Firn Air Sampling, 2001

In January 2001, CMDL scientists joined investigators from Bowdoin University, Princeton University, and the University of Wisconsin to collect an archive of 20th century air from the firn (snowpack) at South Pole (Figure 5.42). Samples were collected into separate pairs of 3-L glass flasks for measurements of O_2/N_2 (by Bowdoin and Princeton) and carbon cycle gases (by CMDL/CCGG); individual 3-L stainless-steel and glass flasks for measurements of halocarbons, N_2O, SF_6, and COS; large (33-L) stainless-steel canisters to maintain an archive of air for future analyses; and a few canisters each for measurement of $^{14}CH_4$ (by NIWA and CSIRO) and very low-level analyses of SF_6 (by Scripps Institution of Oceonograpy, SIO) (Table 5.9). All samples were analyzed during 2001, including initial analyses of the archive canisters. Although it was hoped to obtain air dating back to the turn of the century, the analyses suggest that the earliest date was 1921 for CO_2 and just after 1900 for gases that diffuse more slowly, such as methyl bromide and methyl chloride.

CMDL scientists have been participating in the collection and analysis of firn air from Antarctica and Greenland since 1995. Samples have been analyzed from Vostok, Taylor Dome, South Pole, and Siple Dome in Antarctica and from Tunu in Greenland. The data have been used to estimate the atmospheric histories of these gases where real-time measurements were not available [*Battle et al.*, 1996; *Butler et al.*, 1999], extending the earliest records of many trace gases from the late 1970s back to the end of the 19th century. They also have been used to evaluate seasonal biasing of the mean gas mixing ratios [*Severinghaus et al.*, 2001]. The 2001 sampling at South Pole was the second deep sampling conducted at that site; the first was in 1995. Samples from this most recent collection provide a unique opportunity to examine the diffusion of trace gases in the firn (Figures 5.43 and 5.44), which should reduce error in the estimation of the age of the firn air. Also, the oldest firn air ever collected comes from South Pole, which makes the archived samples particularly valuable for future analyses of gases not yet reported.

Fig. 5.42. Bladder being sent down into one of the two holes at South Pole for subsequent sampling of firn air. The 10-m-long bladder was pressurized to inhibit airflow from above while firn air was sampled through a 15-cm-high, stainless-steel-lined open chamber situated between the bottom of the bladder and the bottom of the hole. Each of two holes, extending ultimately to the snow-ice transition at 122-m depth, was drilled and sampled at 2- to 10-m increments. The drill lies on the snow to the left.

Preliminary evaluation of the data from the 2001 campaign shows that diffusion rates of gases in the firn are very close to molecular rates, calculated by extrapolation of measurements made at very high temperatures to the temperature of the firn, ~ −50 °C. Although often used in models of firn air movement, such extrapolated values are always suspect. Determination of the actual diffusion rates in the firn will remove this uncertainty and allow for the direct calculation of gas diffusion at these temperatures and, subsequently, the mean age of the air at each depth.

TABLE 5.9. Gases Measured in South Pole Firn Air, 2001

Institution	Gas
CMDL or Univ. of Colorado	CO_2, CO, CH_4, N_2O, H_2, SF_6, CFCs, HCFCs, HFC-134a, CH_3Br, CH_3Cl, CH_3I, COS, halons, $^{13}CO_2$
Princeton Univ. or SIO	$^{15}N_2O$, $N_2{}^{18}O$, $^{15}N_2$, $^{18}O_2$, $^{17}O_2$, $^{14}CO_2$, Ar, Kr, Xe, Ne, Ar/N_2, O_2/N_2, SF_6
NIWA or CSIRO	$^{14}CH_4$

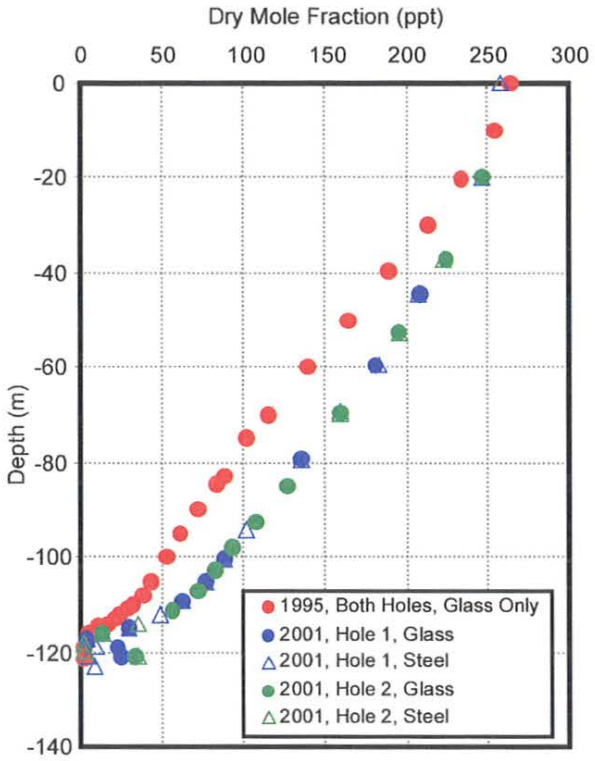

Fig. 5.43. CFC-11 in South Pole firn air in 1995 and 2001. Samples in 1995 were collected from two separate holes, but only into glass flasks. Samples in 2001 also were collected from two separate holes, but both glass and electropolished stainless-steel flasks were used. Note the lower value at the surface in 2001, reflecting the decreased atmospheric burden between 1995 and 2001. Also note the 20-m penetration at mid-depth, where the gradient is steepest and vertical restriction still low.

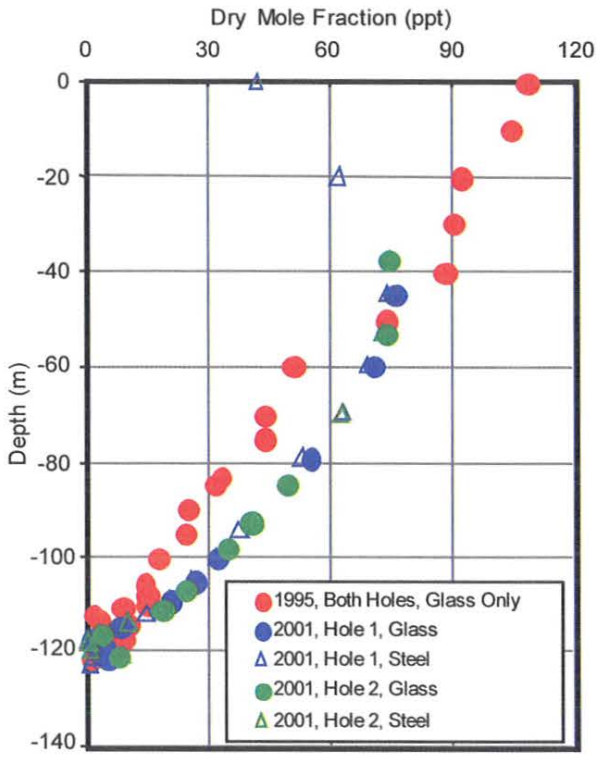

Fig. 5.44. CH_3CCl_3 in South Pole firn air in 1995 and 2001. The 1995 sampling suffered from contamination in the glass flasks, which compromises the interpretation of some of the data points. The 2001 sampling was apparently free of contamination. Note not only the penetration that is similar to that of CFC-11 (Figure 5.43), but also the evidence for the stark turnaround in the CH_3CCl_3 trend in the atmosphere. The turnover occurred in about 1994 in the southern hemisphere, which was an insufficient time lag for this signal to be recorded in the firn in 1995. (The northern hemispheric turnover, in about 1993, was recorded in Greenland firn as early as 1996 [*Butler et. al.*, 1999].) By 2001, the peak of CH_3CCl_3 had penetrated to 45-m depth.

Data are being analyzed and evaluated with the objectives to (1) improve estimates of trace gas diffusion at low temperatures and the corresponding effect on mean-age estimates for firn air samples and (2) report 20th century histories of gases, such as COS, previously not analyzed throughout the century. Other laboratories are currently analyzing the archive of air in 33-L canisters in an attempt to obtain reliable records of additional gases. It is anticipated that sufficient air will be available for analysis of even more gases and isotopes as new analytical techniques become available.

5.6. References

Anderson, J., J.M. Russell III, S. Solomon, and L.E. Deaver, Halogen Occulation Experiment confirmation of stratospheric chlorine decreases in accordance with the Montreal Protocol, *J. Geophys. Res., 105*, 4483-4490, 2000.

Andrews, A.E., K.A. Boering, S.C. Wofsy, B.C. Daube, D.B. Jones, S. Alex, M. Loewenstein, J.R. Podolske, and S.E. Strahan, Empirical age spectra for the midlatitude lower stratosphere from in situ observations of CO_2: Quantitative evidence for a subtropical "barrier" to horizontal transport, *J. Geophys. Res., 106*, 10,257-10,274, 2001.

Andrews, A.E., K.A. Boering, B.C. Daube, S.C. Wofsy, M. Loewenstein, H. Jost, J.R. Podolske, R.L. Herman, R.D. May, E.J. Moyer, J.W. Elkins, G.S. Dutton, D.F. Hurst, F.L. Moore, E.A. Ray, P.A. Romashkin, P.R. Wamsley, and S.E. Strahan, Mean ages of stratospheric air derived from in situ observations of CO_2, CH_4, and N_2O, *J. Geophys. Res.*, in press, 2002.

Battle, M., M. Bender, T. Sowers, P.P. Tans, J.H. Butler, J.W. Elkins, J.T. Ellis, T. Conway, N. Zhang, P. Lang, and A.D. Clarke, Atmospheric gas concentrations over the past century measured in air from firn at the South Pole, *Nature, 383*, 231-235, 1996.

Bergamaschi, P., C.A.M. Brenninkmeijer, M. Hahn, T. Röckmann, D.H. Scharffe, P.J. Crutzen, N.F. Elansky, I.B. Belikov, N.B.A. Trivett, and D.E.J. Worthy, Isotope analysis based source identification for atmospheric CH_4 and CO sampled across

Russia using the trans-Siberian railroad, *J. Geophys. Res., 103*, 8227-8235, 1998.

Butler, J.H., Better budgets for methyl halides?, *Nature, 403*, 260-261, 2000.

Butler, J.H., S.A. Montzka, A.D. Clarke, J.M. Lobert, and J.W. Elkins, Growth and distribution of halons in the atmosphere, *J. Geophys. Res., 103*, 1503-1511, 1998.

Butler, J.H., M. Battle, M. Bender, S.A. Montzka, A.D. Clarke, E.S. Saltzman, C. Sucher, J. Severinghaus, and J.W. Elkins, A twentieth century record of atmospheric halocarbons in polar firn air, *Nature, 399*, 749-765, 1999.

Crutzen, P.J., N.F. Elansky, M. Hahn, G.S. Golitsyn, C.A.M. Brenninkmeijer, D.H. Scharffe, I.B. Belikov, M. Maiss, P. Bergamaschi, T. Röckmann, A.M. Grisenko, and V.M. Sevostyanov, Trace gas measurements between Moscow and Vladivostok using the trans-Siberian railroad, *J. Atmos. Chem., 29*, 179-194, 1998.

Daniel, J.S., S. Solomon, and D.L. Albritton, On the evaluation of halocarbon radiative forcing and global warming potentials, *J. Geophys. Res., 100*, 1271-1285, 1995.

Daniel, J.S., S. Solomon, R.W. Portmann, and R.R. Garcia, Stratospheric ozone destruction: The importance of bromine relative to chlorine, *J. Geophys. Res., 104*, 23,871-23,880, 1999.

Elkins, J.W., Trends of trace gases, total chlorine, and total bromine in the lower stratosphere from 1991 through 2000, *Eos Trans. AGU, 81*, F88, 2000.

Fahey, D.W., K.K. Kelly, G.V. Ferry, L.R. Poole, J.C. Wilson, D.M. Murphy, M. Loewenstein, and K.R. Chan, In situ measurements of total reactive nitrogen, total water, and aerosol in a polar stratospheric cloud in the Antarctic, *J. Geophys. Res., 94*, 11,299-11,315, 1989.

Fahey, D.W., R.S. Gao, K.S. Carslaw, J. Kettleborough, P.J. Popp, M.J. Northway, J.C. Holecek, S.C. Ciciora, R.J. McLaughlin, T.L. Thompson, R.H. Winkler, D.G. Baumgardner, B. Gandrud, P.O. Wennberg, S. Dhaniyala, K. McKinney, T. Peter, R.J. Salawitch, T.P. Bui, J.W. Elkins, C.R. Webster, E.L. Atlas, H. Jost, J.C. Wilson, R.L. Herman, A. Kleinböhl, and M. von König, The detection of large HNO_3-containing particles in the winter Arctic stratosphere, *Science, 291*, 1026-1031, 2001.

Fraser, P.J., D.E. Oram, C.E. Reeves, S.A. Penkett, and A. McCulloch, Southern hemispheric halon trends (1978-1998) and global halon emissions, *J. Geophys. Res., 104*, 15,985-15,999, 1999.

Gan, J., S.R. Yates, H.D. Ohr, and J.J. Sims, Production of methyl bromide by terrestrial higher plants, *Geophys. Res. Lett., 25*, 3595-3598, 1998.

Gao, R.S, E.C. Richard, P.J. Popp, G.C. Toon, D.F. Hurst, P.A. Newman, J.C. Holecek, M.J. Northway, D.W. Fahey, M.Y. Danilin, B. Sen, K. Aikin, P.A. Romashkin, J.W. Elkins, C.R. Webster, S.M. Schauffler, J.B. Greenblatt, C.T. McElroy, L.R. Lait, T.P. Bui, and D. Baumgardener, Observational evidence for the role of denitrification in Arctic stratospheric ozone loss, *Geophys. Res. Lett., 28*, 2879-2882, 2001.

Geller, L.S., J.W. Elkins, J.M. Lobert, A.D. Clarke, D.F. Hurst, J.H. Butler, and R.C. Myers, Tropospheric SF_6: Observed latitudinal distribution and trends, derived emissions, and interhemispheric exchange time, *Geophys. Res. Lett., 24*, 675-678, 1997.

Greenblatt, J.B., H. Jost, M. Loewenstein, J.R. Podolske, T.P. Bui, D.F. Hurst, J.W. Elkins, R.L. Herman, C.R. Webster, S.M. Schauffler, E.A. Atlas, P.A. Newman, L.R. Lait, M. Müller, A. Engel, and U. Schmidt, Definining the polar vortex edge from an N_2O:potential temperature correlation, *J. Geophys. Res.*, in press, 2002.

Grooss, J.-U., G. Günther, P. Konopka, R. Müller, D.S. McKenna, F. Stroh, B. Vogel, A. Engel, M. Müller, K. Hoppel, R. Bevilacqua, E. Richard, R.M. Stimpfle, C.R. Webster, J.W. Elkins, D.F. Hurst, and P.A. Romashkin, Simulation of ozone depletion in spring 2000 with the Chemical Lagrangian Model of the Stratosphere (CLaMS), *J. Geophys. Res.*, in press, 2002.

Groszko, W., and R.M. Moore, Ocean-atmosphere exchange of methyl bromide: NW Atlantic and Pacific Ocean studies, *J. Geophys. Res., 103*, 16,737-16,741, 1998.

Hall, B.D., J.W. Elkins, J.H. Butler, S.A. Montzka, T.M. Thompson, L. Del Negro, G.S. Dutton, D.F. Hurst, D.B. King, E.S. Kline, L. Lock, D. MacTaggart, D. Mondeel, F.L. Moore, J.D. Nance, E.A. Ray, and P.A. Romashkin, Halocarbons and other atmospheric trace species, in *Climate Monitoring and Diagnostics Laboratory Summary Report No. 25 1998-1999*, edited by R.C. Schnell, D.B. King, and R.M. Rosson, pp. 91-113, NOAA Oceanic and Atmos. Res., Boulder, CO, 2001.

Hall, T.M., and R.A. Plumb, Age as a diagnostic of stratospheric transport, *J. Geophys. Res., 99*, 1059-1070, 1994.

Herman, R.L., K. Drdla, J.R. Spackman, D.F. Hurst, C.R. Webster, J.W. Elkins, E.M. Weinstock, J.G. Anderson, B.W. Ganrud, G.C. Toon, M.R. Schoeberl, A.E. Andrews, S.C. Wofsy, H. Jost, E.L. Atlas, D.W. Fahey, and T.P. Bui, Hydration, dehydration, and the total hydrogen budget of the 1999-2000 winter Arctic stratosphere, *J. Geophys. Res.*, in press, 2002.

Hurst, D.F., P.S. Bakwin, R.C. Meyers, and J.W. Elkins, Behavior of trace gas mixing ratios on a very tall tower in North Carolina, *J. Geophys. Res., 102*, 8825-8835, 1997.

Hurst, D.F., G.S. Dutton, P.A. Romashkin, J.W. Elkins, R.L. Herman, E.J. Moyer, D.C. Scott, R.D. May, C.R. Webster, J. Grecu, M. Loewenstein, and J.R. Podolske, Comparison of in situ N_2O and CH_4 measurements in the upper troposphere and lower stratosphere during STRAT and POLARIS, *J. Geophys. Res., 105*, 19,811-19,822, 2000.

Hurst, D.F., S.M. Schauffler, J.B. Greenblatt, H. Jost, R.L. Herman, J.W. Elkins, P.A. Romashkin, E.L. Atlas, S.G. Donnelly, J.R. Podolske, M. Loewenstein, C.R. Webster, G.J. Flesch, and D.C. Scott, The construction of a unified, high-resolution nitrous oxide data set for ER-2 flights during SOLVE, *J. Geophys. Res.*, in press, 2002.

King, D.B., J.H. Butler, S.A. Montzka, S.A. Yvon-Lewis, and J.W. Elkins, Implications of methyl bromide supersaturations in the temperate North Atlantic Ocean, *J. Geophys. Res., 105*, 19,763-19,769, 2000.

Kjellström, E., A three-dimensional global model study of carbonyl sulfide in the troposphere and the lower stratosphere, *J. Atmos. Chem., 29*, 151-177, 1998.

Kurylo, M.J., J.M. Rodriguez, M.O. Andreae, E.L. Atlas, D.R. Blake, J.H. Butler, S. Lal, D.J. Lary, P.M. Midgley, S.A. Montzka, P.C. Novelli, C.E. Reeves, P.G. Simmonds, L.P. Steele, W.T. Sturges, R.F. Weiss, and Y. Yokouchi, Short-lived ozone-related compounds, in *Scientific Assessment of Ozone Depletion: 1998, Global Ozone Res. and Monit. Proj. Rep. 44*, pp. 2.1-2.56, World Meteorol. Org., Geneva, 1999.

Levitus, S., Climatological atlas of the world ocean, *NOAA Prof. Pap., 13*, U.S. Govt. Print. Off., Washington, DC, 1982.

Lobert, J.M., J.H. Butler, S.A. Montzka, L.S. Geller, R.C. Myers, and J.W. Elkins, A net sink for atmospheric CH_3Br in the East Pacific Ocean, *Science, 267*, 1002-1005, 1995.

Lobert, J.M., J.H. Butler, L.S. Geller, S.A. Yvon, S.A. Montzka, R.C. Myers, A.D. Clarke, and J.W. Elkins, BLAST94: Bromine Latitudinal Air/Sea Transect 1994: Report on oceanic measurements of methyl bromide and other compounds, *NOAA Tech. Memo. ERL CMDL-10*, 39 pp., NOAA Oceanic and Atmos. Res., Boulder, CO, 1996.

Lobert, J.M., S.A. Yvon-Lewis, J.H. Butler, S.A. Montzka, and R.C. Myers, Undersaturation of CH_3Br in the Southern Ocean, *Geophys. Res. Lett., 24*, 171-172, 1997.

Montzka, S.A., J.H. Butler, R.C. Myers, T.M. Thompson, T.H. Swanson, A.D. Clarke, L.T. Lock, and J.W. Elkins, Decline in the tropospheric abundance of halogen from halocarbons: Implications for stratospheric ozone depletion, *Science, 272*, 1318-1322, 1996.

Montzka, S.A., J.H. Butler, J.W. Elkins, T.M. Thompson, A.D. Clarke, and L.T. Lock, Present and future trends in the atmospheric burden of ozone-depleting halogens, *Nature, 398*, 690-694, 1999.

Montzka, S.A., C.M. Spivakovsky, J.H. Butler, J.W. Elkins, L.T. Lock, and D.J. Mondeel, New observational constraints for atmospheric hydroxyl on global and hemispheric scales, *Science, 288*, 500-503, 2000.

Moore, F.L., J.W. Elkins, E.A. Ray, G.S. Dutton, R.E. Dunn, D.W. Fahey, R.J. McLaughlin, T.L. Thompson, P.A. Romashkin, D.F. Hurst, and P.R. Wamsley, Balloonborne in situ gas chromatograph for measurements in the troposphere and stratosphere, *J. Geophys. Res.*, in press, 2002.

Morgenstern, O., J.A. Pyle, A. Iwi, W.A. Norton, J.W. Elkins, D.F. Hurst, and P.A. Romashkin, On the diagnosis of mixing from tracer-tracer correlations, 2, Comparison of model and measurements, *J. Geophys. Res.*, in press, 2002.

Morris, R.A., T.M. Miller, A.A. Viggiano, J.F. Paulson, S. Solomon, and G. Reid, Effects of electron and ion reactions on atmospheric lifetimes of fully fluorinated compounds, *J. Geophys. Res., 100*, 1287-1294, 1995.

Oberlander, E.A., C.A.M. Brenninkmeijer, P.J. Crutzen, N.F. Elansky, G.S. Golitsyn, I.G. Granberg, D.H. Scharffe, R. Hofmann, I.B. Belikov, H.G. Paretzke, and P.F.J. van Velthoven, Trace gas measurements along the trans-Siberian railroad: The TROICA 5 expedition, *J. Geophys. Res.*, in press, 2002.

Plumb, R.A., D.W. Waugh, and M.P. Chipperfield, The effects of mixing on tracer relationships in the polar vortices, *J. Geophys. Res., 105*, 10,047-10,062, 2000.

Popp, P.J., M.J. Northway, J.C. Holecek, R.S. Gao, D.W. Fahey, J.W. Elkins, D.F. Hurst, P.A. Romashkin, G.C. Toon, B. Sen, S.M. Schauffler, R.J. Salawitch, C.R. Webster, R.L. Herman, H. Jost, T.P. Bui, P.A. Newman, and L.R. Lait, Severe and extensive denitrification in the 1999-2000 Arctic winter stratosphere, *Geophys. Res. Lett., 28*, 2875-2878, 2001.

Prinn, R.G., R. Zander, D.M. Cunnold, J.W. Elkins, A. Engel, P.J. Fraser, M.R. Gunson, M.K.W. Ko, E. Mahieu, P.M. Midgley, J.M. Russell III, C.M. Volk, and R.F. Weiss, Long-lived ozone-related compounds, in *Scientific Measurement of Ozone Depletion: 1998, Global Ozone Res. and Monit. Proj. Rep. 44*, pp. 1.1-1.54, World Meteorol. Org., Geneva, 1999.

Prinn, R.G., J. Huang, R.F. Weiss, D.M. Cunnold, P.J. Fraser, P.G. Simmonds, A. McCulloch, C. Harth, P. Salameh, S. O'Doherty, R.H.J. Wang, L. Porter, and B.R. Miller, Evidence for substantial variations of atmospheric hydroxyl radicals in the past two decades, *Science, 292*, 1882-1888, 2001.

Proffitt, M.H., and R.C. McLaughlin, Fast-response dual-beam UV-absorption ozone photometer suitable for use in stratospheric balloons, *Rev. Sci. Instrum., 54*, 1719-1728, 1983.

Ray, E.A., F.L. Moore, J.W. Elkins, D.F. Hurst, P.A. Romashkin, G.S. Dutton, and D.W. Fahey, Descent and mixing in the northern polar vortex from in situ tracer measurements, *J. Geophys. Res.*, in press, 2002.

Redeker, K.R., N.-Y. Wang, J.C. Low, A. McMillan, S.C. Tyler, and R.J. Cicerone, Emissions of methyl halides and methane from rice paddies, *Science, 290*, 966-969, 2000.

Rex, M., et al., Chemical depletion of Arctic ozone in winter 1999/2000, *J. Geophys. Res.*, in press, 2002.

Rhew, R.C., B.R. Miller, and R.F. Weiss, Natural methyl bromide and methyl chloride emissions from coastal salt marshes, *Nature, 403*, 292-295, 2000.

Rhew, R.C., B.R. Miller, M.K. Vollmer, and R.F. Weiss, Shrubland fluxes of methyl bromide and methyl chloride, *J. Geophys. Res., 106*, 20,875-20,882, 2001.

Richard, E.C., K. Aikin, A. Andrews, B.C. Daube, C. Gerbig, S.C. Wofsy, P.A. Romashkin, D.F. Hurst, J.W. Elkins, E.A. Ray, F.L. Moore, T. Deschler, and G.C. Toon, Severe chemical ozone loss inside the Arctic polar vortex during winter 1999-2000 inferred from in situ airborne measurements, *Geophys. Res. Lett., 28*, 2197-2200, 2001.

Romashkin, P.A., D.F. Hurst, J.W. Elkins, G.S. Dutton, and P.R. Wamsley, Effect of the tropospheric trend on the stratospheric tracer-tracer correlations: Methyl chloroform, *J. Geophys. Res., 104*, 26,643-26,652, 1999.

Romashkin, P.A., D.F. Hurst, J.W. Elkins, G.S. Dutton, D.W. Fahey, R.E. Dunn, F.L. Moore, R.C. Myers, and B.D. Hall, In situ measurements of long-lived trace gases in the lower stratosphere by gas chromatography, *J. Atmos. Oceanic Technol., 18*, 1195-1204, 2001.

Salawitch, R.J., J.J. Margitan, B. Sen, G.C. Toon, G.B. Osterman, M. Rex, J.W. Elkins, E.A. Ray, F.L. Moore, D.F. Hurst, P.A. Romashkin, R.M. Bevilacqua, K. Hoppel, E.C. Richard, and T.P. Bui, Chemical loss of ozone during the Arctic winter of 1999-2000: An analysis based on balloon-borne observations, *J. Geophys. Res.*, in press, 2002.

Schauffler, S.M., E.L. Atlas, D.R. Blake, F. Flocke, R.A. Lueb, J.M. Lee-Taylor, V. Stroud, and W. Travnicek, Distributions of brominated organic compounds in the troposphere and lower stratosphere, *J. Geophys. Res., 104*, 21,513-21,535, 1999.

Schauffler, S.M., E.L. Atlas, S.G. Donnelly, A.E. Andrews, S.A. Montzka, J.W. Elkins, D.F. Hurst, P.A. Romashkin, and V. Stroud, Chlorine budget and partitioning during SOLVE, *J. Geophys. Res.*, in press, 2002.

Schnell, R.C., D.B. King, and R.M. Rosson (Eds.), *Climate Monitoring and Diagnostics Laboratory Summary Report No. 25 1998-1999*, 154 pp., NOAA Oceanic and Atmos. Res., Boulder, CO, 2001.

Severinghaus, J.P., A. Grachev, and M. Battle, Thermal fractionation of air in polar firn by seasonal temperature gradients, *Geochem. Geophys. Geosyst., 2*, paper number 2000GC000146 (electronic journal), 2001.

Solomon, S., D. Wuebbles, I. Isaksen, J. Kiehl, M. Lal, P. Simon, and N.-D. Sze, Ozone depletion potentials, global warming potentials, and future chlorine/bromine loading, in *Scientific Assessment of Ozone Depletion: 1994, Global Ozone Res. and Monit. Proj. Rep. 37*, pp. 13.1-13.36, World Meteorol. Org., Geneva, 1995.

Sturges, W.T., D.E. Oram, L.J. Carpenter, S.A. Penkett, and A. Engel, Bromoform as a source of stratospheric bromine, *Geophys. Res. Lett., 27*, 2081-2084, 2000.

Tans, P.P, P.S. Bakwin, L. Bruhwiler, T.J. Conway, E.J. Dlugokencky, D.W. Guenther, D.R. Kitzis, P.M. Lang, K.A. Masarie, J.B. Miller, P.C. Novelli, K.W. Thoning, M. Trudeau, B.H. Vaughn, J.W.C. White, and C. Zhao, Carbon cycle, in *Climate Monitoring and Diagnostics Laboratory Summary Report No. 25 1998-1999*, edited by R.C. Schnell, D.B. King, and R.M. Rosson, pp. 24-46, NOAA Oceanic and Atmos. Res., Boulder, CO, 2001.

UNEP (United Nations Environmental Programme), *Montreal Protocol on Substances that Deplete the Ozone Layer: Final Act,* 15 pp., New York, 1987.

Varner, R.K., P.M. Crill, and R.W. Talbot, An estimate of the uptake of atmospheric methyl bromide by agricultural soils, *Geophys. Res. Lett., 26*, 727-730, 1999.

Volk, C.M., J.W. Elkins, D.W. Fahey, G.S. Dutton, J.M. Gilligan, M. Loewenstein, J.R. Podolske, K.R. Chan, and M.R. Gunson, Evaluation of source gas lifetimes from stratospheric observations, *J. Geophys. Res., 102*, 25,543-25,564, 1997.

Wamsley, P.R., J.W. Elkins, D.W. Fahey, G.S. Dutton, C.M. Volk, R.C. Myers, S.A. Montzka, J.H. Butler, A.D. Clarke, P.J. Fraser, L.P. Steele, M.P. Lucarelli, E.L. Atlas, S.M. Schauffler, D.R. Blake, F.S. Rowland, W.T. Sturges, J.M. Lee, S.A. Penkett, A. Engel, R.M. Stimpfle, K.R. Chan, D.K. Weisenstein, M.K.W. Ko, and R.J. Salawitch, Distribution of halon-1211 in the upper troposphere and lower stratosphere and the 1994 total bromine budget, *J. Geophys. Res., 103*, 1513-1526, 1998.

Woodbridge, E.L., J.W. Elkins, D.W. Fahey, L.E. Heidt, S. Solomon, T.J. Baring, T.M. Gilpin, W.H. Pollock, S.M. Schauffler, E.L. Atlas, M. Loewenstein, J.R. Podolske, C.R. Webster, R.D. May, J.M. Gilligan, S.A. Montzka, K.A. Boering, and R.J. Salawitch, Estimates of total organic and inorganic chlorine in the lower stratosphere from in situ and flask measurements, *J. Geophys. Res., 100*, 3057-3064, 1995.